Tracing the origin and core formation of the enstatite achondrite parent bodies using Cr isotopes

Frédéric Moynier, Martin Schiller, Harry Becker, Jean-Alix Barrat, Martin Bizzarro

▶ **To cite this version:**

Frédéric Moynier, Martin Schiller, Harry Becker, Jean-Alix Barrat, Martin Bizzarro. Tracing the origin and core formation of the enstatite achondrite parent bodies using Cr isotopes. Geochimica et Cosmochimica Acta, 2021, 308 (9), pp.256-272. 10.1016/j.gca.2021.05.053 . hal-03840853

HAL Id: hal-03840853
https://hal.science/hal-03840853

Submitted on 2 Aug 2023

HAL is a multi-disciplinary open access archive for the deposit and dissemination of scientific research documents, whether they are published or not. The documents may come from teaching and research institutions in France or abroad, or from public or private research centers.

L'archive ouverte pluridisciplinaire **HAL**, est destinée au dépôt et à la diffusion de documents scientifiques de niveau recherche, publiés ou non, émanant des établissements d'enseignement et de recherche français ou étrangers, des laboratoires publics ou privés.

Distributed under a Creative Commons Attribution - NonCommercial 4.0 International License

Version of Record: https://www.sciencedirect.com/science/article/pii/S0016703721003343
Manuscript_ee9f90178fdabbdc96f986ed36538782

Tracing the origin and core formation of the enstatite achondrite parent bodies using Cr isotopes

Ke Zhu (朱柯)[1,3*], Frédéric Moynier[1], Martin Schiller[2], Harry Becker[3], Jean-Alix Barrat[4], Martin Bizzarro[1,2]

[1]Université de Paris, Institut de Physique du Globe de Paris, CNRS, 75005, Paris France

[2]Centre for Star and Planet Formation, Globe Institute, University of Copenhagen, Øster Voldgade 5–7, Copenhagen DK-1350, Denmark

[3]Freie Universität Berlin, Institut für Geologische Wissenschaften, Malteserstr. 74-100, 12249 Berlin, Germany

[4]Univ. Brest, CNRS, UMR 6539 (Laboratoire des Sciences de l'Environnement Marin), LIA BeBEST, Institut Universitaire Européen de la Mer (IUEM), Place Nicolas Copernic, 29280 Plouzané, France.

*corresponding author: zhu@ipgp.fr

R2 revision resubmitted to GCA on May 26th, 2021

© 2021 published by Elsevier. This manuscript is made available under the CC BY NC user license
https://creativecommons.org/licenses/by-nc/4.0/

Abstract:

Enstatite achondrites (including aubrites) are the only differentiated meteorites that have similar isotope compositions to the Earth-Moon system for most of the elements. However, the origin and differentiation of enstatite achondrites and their parent bodies remain poorly understood. Here, we report high-precision mass-independent and mass-dependent Cr isotope data for 10 enstatite achondrites, including eight aubrites, Itqiy and one enstatite-rich clast in Almahatta Sitta, to further constrain the origin and evolution of their parent bodies. The ε^{54}Cr (per 10,000 deviation of the mass bias corrected $^{54}Cr/^{52}Cr$ ratio from a terrestrial standard) systematics define three groups: main-group aubrites with $\varepsilon^{54}Cr = 0.06 \pm 0.12$ (2SD, N =7) that is similar to the enstatite chondrites and the Earth-Moon system, Shallowater aubrite with $\varepsilon^{54}Cr = -0.12 \pm 0.04$ and Itqiy-type meteorites with $\varepsilon^{54}Cr = -0.26 \pm 0.03$ (2SD, N =2). This shows that there were at least three enstatite achondrite parent bodies in the Solar System. This is confirmed by their distinguished mass-dependent Cr isotope compositions (δ^{53}Cr values): 0.24 ± 0.03 ‰, 0.10 ± 0.03 ‰ and -0.03± 0.03 ‰ for main-group, Shallowater and Itqiy parent bodies, respectively. Aubrites are isotopically heavier than chondrites ($\delta^{53}Cr = -0.12 \pm 0.04$ ‰), which likely results from the formation of an isotopically light sulfur-rich core. We also obtained the abundance of the radiogenic ^{53}Cr (produced by the radioactive decay of ^{53}Mn, $T_{1/2}$= 3.7 million years). The radiogenic ε^{53}Cr excesses correlate with the $^{55}Mn/^{52}Cr$ ratios for aubrites

41 (except Shallowater and Bustee) and also the Cr stable isotope compositions (δ^{53}Cr
42 values). We show that these correlations represent mixing lines that also hold
43 chronological significance since they are controlled by the crystallization of sulfides
44 and silicates, which mostly reflect the main-group aubrite parent body differentiation
45 at 4562.5 ± 1.1 Ma (i.e., 4.8 ± 1.1 Ma after Solar System formation). Furthermore, the
46 intercept of these lines with the ordinate axis which represent the initial ε^{53}Cr value of
47 main-group aubrites (0.50 ± 0.16, 2σ) is much higher than the average ε^{53}Cr value of
48 enstatite chondrites (0.15 ± 0.10, 2SD), suggesting an early sulfur-rich core formation
49 that effectively increased the Mn/Cr ratio of the silicate fraction of the main-group
50 aubrite parent body.
51

1. Introduction

Enstatite achondrites, e.g., aubrites, are the only differentiated meteorite group that have similar oxygen isotope composition with that of the Earth-Moon system (Clayton et al., 1984; Greenwood et al., 2017). This isotopic similarity also extends to other isotope systems such as Ti, Cr or H, suggesting a close genetic link between the solid precursors of aubrites and the Earth-Moon system (Barrat et al., 2016; Greenwood et al., 2018; Greenwood et al., 2017; Newton et al., 2000; Piani et al., 2020; Trinquier et al., 2007; Zhang et al., 2012), although aubrites have distinct chemical and mineralogical composition and are more reduced than the Earth and the Moon (Keil, 2010a). Aubrites are more akin to the surface of Mercury (Ebel and Alexander, 2011; Nittler and Weider, 2019; Udry et al., 2019; Wasson, 1988). As such, the origin and evolution of aubrites may be closely linked to those of Earth, Moon and Mercury.

In detail, aubrites formed under highly reducing conditions with oxygen fugacities (fO_2) ranging from ~2 to ~6 log units below the iron-wustite (IW) buffer (Keil, 1968, 2010b). They consist predominately of FeO-poor enstatite (75 ~ 98% vol.) and contain minor silicate phases including plagioclase, diopside and forsterite (Watters and Prinz, 1979). Due to their formation under low fO_2 conditions, aubrites contain S-rich accessory minerals, such as troilite (FeS), alabandite (MnS) and oldhamite (CaS). Most aubrites are breccias and appear to originate from one or more parent bodies that underwent extensive melting and differentiation (Keil, 1989). Their highly siderophile

72 elements (HSE) depletion supports the idea that their parent body/bodies underwent
73 core formation (van Acken et al., 2012a; van Acken et al., 2012b).

74 The formation of both aubrites and enstatite chondrites (ECs) occurred under
75 extremely reduced conditions (Keil, 2010b; Lodders et al., 1993) and from precursors
76 with similar isotopic compositions, suggesting a genetic relationship between the two
77 parent bodies (e.g., Lodders et al., 1993; van Acken et al., 2012b). However, other lines
78 of evidence including mineralogy, petrology, elemental abundances and cosmic ray
79 exposure ages are difficult to reconcile with formation of aubrites from an enstatite
80 chondrite precursor [see chapter 9.1 in Keil (2010b)]. Probing their relative genetic
81 relationships may be improved by a better understanding of the chronology of
82 formation of the aubrites, which is currently poorly defined. The lack of a radiogenic
83 ^{26}Mg deficit in aubrites, while they have sub-chondritic ^{27}Al/^{24}Mg ratios, suggests that
84 they formed after the decay of ^{26}Al, i.e. at least 3 million years (Ma) after Solar System
85 formation (Baker et al., 2012). Iodine-Xenon systematics of Shallowater suggests it
86 formed at 4562.4 ± 0.2 Ma (Pravdivtseva et al., 2017). Given that Shallowater is an
87 unusual enstatite achondrite, which likely originates from a distinct parent body
88 relative to other aubrites (Keil, 2010b; Moynier et al., 2011a), the timing of formation
89 of Shallowater cannot be generalized to the main-group aubrites. Thus, the timing of
90 aubrites and aubrite parent body formation remains largely unconstrained.

91 Chromium isotope systematics of aubrites may improve our understanding of the
92 origin of aubrites. 1) The abundance of the neutron-rich isotope ^{54}Cr (nucleosynthetic)

93 varies among different meteorites (Trinquier et al., 2007). This feature, expressed as the
94 ε^{54}Cr (per 10,000 deviation of the mass bias corrected ^{54}Cr/^{52}Cr ratio from to the
95 terrestrial standard NIST SRM 979) signature, has been established as a tracer of the
96 genetic relationships between meteorites (Qin et al., 2010; Trinquier et al., 2007; Zhu
97 et al., 2021b). 2) The radiogenic isotope ^{53}Cr is the daughter product of the short-lived
98 isotope ^{53}Mn (half-life of 3.7 million years (Holden, 1990). This decay system can
99 provide precise relative chronology of early Solar System events while ^{53}Mn was still
100 present (Birck and Allègre, 1988; Lugmair and Shukolyukov, 1998). The ^{53}Mn-^{53}Cr
101 chronometer is especially sensitive to volatilization and magmatic processes, because
102 Mn and Cr possess different volatility and chemical behavior during magmatic
103 differentiation (Lodders, 2003; Sossi et al., 2019). This system has been successfully
104 applied to date the differentiation of other planetary objects, including: Vesta (Lugmair
105 and Shukolyukov, 1998; Trinquier et al., 2008b), angrite (Zhu et al., 2019b) and ureilite
106 parent bodies (Van Kooten et al., 2017; Yamashita et al., 2010; Zhu et al., 2020b). 3)
107 Mass-dependent Cr stable isotope variations (expressed as δ^{53}Cr, the per mil variation
108 of the ^{53}Cr/^{52}Cr ratio relative to the terrestrial standard NIST SRM 979) can be used to
109 trace planetary processes, such as volatile depletion (Sossi et al., 2018; Zhu et al.,
110 2019c), magmatic differentiation (Bonnand et al., 2020a; Bonnand et al., 2020b;
111 Bonnand et al., 2016a; Shen et al., 2019; Sossi et al., 2018; Zhu et al., 2019c), and
112 possibly core formation (Moynier et al., 2011b).

113 So far, the only ε^{54}Cr value of aubrites has been reported for Bishopville (-0.16 ±

114 0.19) (Trinquier et al., 2007). This isotopic composition overlaps with the ε^{54}Cr
115 signatures of enstatite (0.02 ± 0.11; 2SD, N = 13), Rumuruti (-0.06 ± 0.08; 2SD, N =
116 12) and ordinary (-0.39 ± 0.09; 2SD, N = 18) chondrites (Mougel et al., 2018;
117 Pedersen et al., 2019; Qin et al., 2010; Trinquier et al., 2007; Zhu et al., 2021a; Zhu et
118 al., 2021b). Consequently, the currently available ε^{54}Cr datum for aubrite limits its use
119 to test genetic links to chondrites (e.g., enstatite and Rumuruti chondrites with ε^{54}Cr
120 of ~0) and other achondrites (e.g., martian meteorites and angrites with ε^{54}Cr of ~-0.2
121 and ~-0.4 respectively; Trinquier et al., 2007; Zhu et al., 2019b), as well as possible
122 mantle heterogeneity of the aubrite parent body and whether there are multiple parent
123 bodies for enstatite achondrites (e.g., Zhu et al., 2020b). Shukolyukov and Lugmair
124 (2004) reported ε^{53}Cr values for three bulk aubrites that established a ^{53}Mn-^{53}Cr
125 isochron corresponding to a ^{53}Mn/^{55}Mn initial ratio of (2.0 ± 0.5) × 10^{-6} and an
126 absolute age of 4560.8 ± 1.4 Ma, relative to the U isotope corrected U-Pb age of the
127 D'Orbigny angrite (Amelin, 2008; Brennecka and Wadhwa, 2012; Glavin et al., 2004).
128 Although the limitation of a three-point isochron makes the age significance of the
129 isochron somewhat uncertain, these data provide promising evidence that Mn-Cr dating
130 could fruitfully be used to better constrain the timing of aubrite formation and
131 differentiation. Combined with Cr stable isotope information, these data may shed
132 more light on the magmatic evolution and differentiation history of the aubrite parent
133 bodies.

134 Aubrites are not the only class of enstatite achondrites. Recently, Harries and

Bischoff (2020) observed a new type of enstatite-rich differentiated meteorite clasts in Almahatta Sitta, which are believed to come from another asteroid with a size of ~500 km. These clasts also show petrological affinity to Itqiy, an EH7-anomalous meteorite, as they both underwent partial melting and are petrologically different from aubrites (Keil and Bischoff, 2008; Moynier et al., 2020; Patzer et al., 2001). The Cr isotope compositions of these different types of enstatite achondrites can be used to test their relationship to each other and to enstatite chondrites. Thus, here we report high-precision mass-independent and mass-dependent Cr isotope data for eight aubrite meteorites, the Itqiy meteorite and one enstatite achondrite clast from Almahatta Sitta.

2. Samples and analytical methods

2.1 Sample description.

The eight aubrites selected for this study are Khor Temiki, Bustee, Norton County, Allan Hills [ALH] A78113, ALH 84007, Larkman Nunatak [LAR] 04316, Shallowater and Cumberland Falls. We also studied two other enstatite-rich achondrite meteorites, Itqiy (EH7-anomalous) and one enstatite-rich clast in Almahatta Sitta, MS-MU-19 (Harries and Bischoff, 2020). Itqiy and MS-MU-19 are enstatite-rich rocks, both of which lack plagioclase and high-Ca pyroxene, suggesting they underwent higher degrees of partial melting. Their detailed petrology are described in Patzer et al. (2001) and Harries and Bischoff (2020), respectively. The fractions of Itqiy and MS-MU-19 that we used had been previously partially processed and leached by hot (120°C) 6N HCl in order to remove metal and sulfides for trace element studies. While a fraction of the Cr must have been lost during this process, the Cr of the acid residues that we obtained (mostly from the silicates) likely represent the primitive ε^{54}Cr value, since enstatite is the major Cr-host of these samples and magmatic process would have had homogenized the ε^{54}Cr signatures at the meteorite scale in any cases. We also dissolved a bulk Itqiy from another chip for mass-dependent Cr isotope study.

2.2 Sample dissolution

Small fragments of eight aubrite meteorites were crushed to powders using an agate mortar. From this powdered material, 30–50 mg were transferred into Teflon

bombs for digestion. We also dissolved a small chip (26.4 mg) of LAR 04316 for a replicate. Samples were dissolved following the protocol described in Inglis et al. (2018) using Teflon bombs and an Analab EvapoClean, which has been successfully applied in previous Cr isotopic studies of meteorites (Zhu et al., 2019b; Zhu et al., 2020b). The procedure involved heating in concentrated HF and HNO_3 (2:1) at 140 °C for two days, and subsequent dissolution in 6N HCl (also at 140 °C) for another two days to ensure complete digestion of fluorides, and refractory phases such as chromite and spinel. After complete digestion a ~2% aliquot was used for determination of the $^{55}Mn/^{52}Cr$ ratios and major element contents by ICP-MS in IPGP, ~50% of the digestion were purified for Cr by the following four-step column chemistry described in (Zhu et al., 2021b) for mass-independent Cr isotopic analyses, and the residual 40% were spiked with a ^{50}Cr-^{54}Cr double spike before a two-step column Cr purification for mass-dependent Cr isotopic analyzes of which method is described in the literature (Sossi et al., 2018; Zhu et al., 2021a; Zhu et al., 2019c).

2.3 Mass–independent Cr isotope ($\varepsilon^{53}Cr$ and $\varepsilon^{54}Cr$) analyses

We first used an anion chromatographic purification scheme to efficiently remove Fe from the remaining sample in 6M HCl, followed by elution of Cr on a 1-mL cation exchange column in 20 mL of 0.5M HNO_3 to remove the major elements including Mg, Ca, Al, Ni (Bizzarro et al., 2011) and collect all the Cr species (major Cr^0 and minor Cr^{2+} and Cr^{3+}) to reach a ~100% recovery. Prior to sample loading on the cation column, we used a Cr pre-treatment procedure involving dissolution in 10M HCl at >120 °C to

efficiently promote the formation of Cr(III)-Cl species, which have a low affinity for the cation exchanger and thus elutes early (Larsen et al., 2016; Trinquier et al., 2008a). The third clean-up column involved Cr purification from Al, Fe, V, Ti (and other high-field-strength elements) and Na, K on a small (0.33ml) cation exchange column using 0.5M HNO_3, 1M HF and 6M HCl (Larsen et al., 2018). Prior to sample loading onto this last column, we used a Cr pre-treatment procedure involving exposure to 0.5M HNO_3 + 0.6% H_2O_2 at room temperature for >1 day to promote the formation of Cr^{3+} (Larsen et al. 2016). However, it is difficult to transform all the Cr to Cr^{3+}, so we collect the Cr^0 in 0.5 ml solution of sample loading and 0.5 mL 0.5N HNO_3 elution to increase the recovery to >95% in this column. Finally, in the fourth column, 0.7 mL of TODGA resin were used in 8N HCl to remove the residual Fe, V and Ti which are isobars for ^{54}Cr (^{54}Fe) and ^{50}Cr (^{50}V and ^{50}Ti) (Pedersen et al., 2019). The four columns can reach a total yield between 95% and 99%, and effectively remove Fe, V and Ti, which benefits the isotope analysis on MC-ICPMS. The total blank of <5 ng is negligible compared to the 5-20 μg of Cr processed through the columns. The final Cr solution was re-dissolved in 100μL of concentrated HNO_3 and then dried again 2-3 times to transform the acid media and to minimize residual organics (i.e. from the cation exchange resin).

The $^{55}Mn/^{52}Cr$ ratios with an uncertainty of 5% were measured on a Neptune plus multiple-collector inductively-coupled-plasma mass-spectrometer (MC-ICP-MS) following the protocol described by (Zhu et al., 2021b) and previously used in (Zhu et

al., 2019b; Zhu et al., 2020b). The Cr isotopic compositions were determined using a Neptune Plus MC-ICP-MS located at the Centre for Star and Planet Formation, Globe Institute, University of Copenhagen. Detailed analytical and data reduction method are described in (Zhu et al., 2021b). Sample solutions with concentration of less than 1 ppm were introduced via an ESI APEX and analyzed at a ^{52}Cr signal of 30-40 V, except for Norton County, with low-Cr content (180 ppm), that was analyzed at 15 V. Each sample was measured five times by sample-standard bracketing relative to the NIST SRM 979 Cr standard. The ^{53}Cr/^{52}Cr and ^{54}Cr/^{52}Cr ratios were normalized to a constant ^{50}Cr/^{52}Cr ratio of 0.051859 using an exponential law (Lugmair and Shukolyukov, 1998) and are expressed in the epsilon notation:

$$\varepsilon^{x}Cr = \left(\frac{\left(^{x}Cr/^{52}Cr\right)_{sample}}{\left(^{x}Cr/^{52}Cr\right)_{NIST\ SRM\ 979}} - 1\right) \times 10000 \quad (1),$$

with x = 53 or 54.

The measurements in this study are performed following Zhu et al. (2021b), and the related elemental doping tests (for Ti, V, Fe, K, and Na), external precision tests and the isotope data of known standard samples for data quality (Allende, DTS-1, PCC-1, DTS-2b) can be also found in Zhu et al. (2021b). The data for the reference standards are consistent with previously reported values (Mougel et al., 2018; Qin et al., 2010; Schiller et al., 2014; Schneider et al., 2020; Trinquier et al., 2007; Trinquier et al., 2008b; Zhu et al., 2019a; Zhu et al., 2019b; Zhu et al., 2020b), confirming the accuracy of our new data.

For acid leachates of Itqiy and the enstatite achondrite clast from Almahatta Sitta (MS-MU-19), the purification followed a two-step cation column as originally described in Trinquier et al. (2008a) and modified in Zhu et al. (2019c). Low-yield (e.g., < 70%) Cr purification may produce large equilibrium mass-dependent Cr isotope fractionation from column chemistry which cannot be well corrected using the exponential law (Qin et al., 2010; Trinquier et al., 2008a). Thus, similar to the method used in Moynier et al. (2011b), we used 3 (1 + 1 + 1) mL of 6M HCl for washing the column and we collected the residual material from the first 1-mL cation column and re-passed them in the first column to ensure yields ranging from 88% to 99% (average of 93%). The blank of the full chemical purification is between 0.5 and 2 ng and is negligible compared to 2 – 4 μg of Cr processed through the purification scheme. The mass-independent Cr isotope analysis was obtained via the total evaporation method on the Triton TIMS housed at Freie Universität Berlin based on methods described in the literature (Van Kooten et al., 2016; Zhu et al., 2019b; Zhu et al., 2020a). NIST 3112a was used as the isotope standard, because there is no resolvable mass-independent Cr isotope difference between NIST SRM 979 and NIST SRM 3112a (Zhu et al., 2021b). Using this method, we also measured the Cr isotope composition from the same dissolution of the Allende meteorite and DTS-1 (terrestrial dunite, USGS terrestrial standard) samples that were used for the MC-ICP-MS analysis, and the data are consistent. The data for individual measurements of TIMS total-evaporation measurements are listed in the Appendix.

2.4 Mass–dependent Cr isotope (δ^{53}Cr) measurements

The procedure for mass–dependent Cr isotope analysis was performed at the IPGP on aliquots of the same dissolutions used for mass–independent isotope measurements. First, the appropriate amount of ^{50}Cr–^{54}Cr double spike (28% of the Cr content endemic to the sample) was added to the aliquot, which was then refluxed in a closed beaker at 120 °C overnight to homogenize the sample and spike (e.g., Wu et al., 2020). The Cr of the samples was chemically purified via a typical two–step cation exchange chromatography (Sossi et al., 2018; Zhu et al., 2021a; Zhu et al., 2019c), modified from Trinquier et al. (2007). This method has a total procedural yield of 60–90% and a blank of ~5 ng of Cr. Compared to the total 3-40 μg of Cr from the samples, the blank can be neglected. The final Cr cut was evaporated in concentrated HNO_3 drops 3 to 5 times to convert the HCl medium to HNO_3 and to remove leftover organics (i.e., the resin) following which the samples were diluted to a concentration of 1 ppm Cr, in 2% (0.317 M) HNO_3 for isotope analysis.

The Cr stable isotope compositions of these purified samples were measured on a Thermo Scientific Neptune Plus MC–ICP–MS housed at the IPGP. Analytical details are described in Zhu et al. (2021a), Sossi et al. (2018) and Zhu et al. (2019c). The purified sample solution was diluted to ~ 1ppm, which returned a signal of ~ 15V of ^{52}Cr with a Stable Introduction System (SIS). Every measurement is composed of 100 cycles, with integration time of 4.194 s for each cycle. The final Cr stable isotope data

(δ^{53}Cr) for aubrites were corrected using their respective mass–independent Cr isotope compositions that had previously been analyzed on the same aliquots. The isotopic ratio for samples is reported in delta notation relative to NIST SRM 979:

$$\delta^{53}Cr(‰) = \left(\frac{(^{53}Cr/^{52}Cr)_{sample}}{(^{53}Cr/^{52}Cr)_{NIST\ SRM\ 979}} - 1\right) \times 1000 \quad (2)$$

The uncertainties quoted are the 2SD of individual sample measurements or the 2SD reproducibility of several NIST SRM 979 measurements in the same analytical session (~0.03 ‰), whichever is the largest. Similarly, the Cr stable isotope compositions of standard samples, including NIST SRM 3112a (unpurified, δ^{53}Cr = -0.08 ± 0.03 ‰; 2SD, N = 5), DTS-1 (δ^{53}Cr = -0.03 ± 0.03 ‰; 2SD, N = 5), PCC-1 (δ^{53}Cr = -0.04 ± 0.03 ‰; 2SD, N = 6) and BHVO-2 (δ^{53}Cr = -0.15 ± 0.03 ‰; 2SD, N = 2), were also measured in this study to test the data quality. Our data are consistent with previous studies (Bonnand et al., 2016b; Liu et al., 2019; Schoenberg et al., 2016; Sossi et al., 2018; Wu et al., 2020; Zhu et al., 2019c), which suggests that our δ^{53}Cr data are accurate to the stated uncertainties.

3. Results

All the sample information, elemental contents, mass-independent (ε^{53}Cr and ε^{54}Cr) and mass-dependent (δ^{53}Cr) Cr isotope data together with literature Cr and O isotope data from Shukolyukov and Lugmair (2004), Barrat et al. (2016), Clayton et al. (1984) and Newton et al. (2000) are reported in Table 1. The ε^{54}Cr variability between the analyzed aubrites is rather limited with six out of the nine aubrites (including two LAP 04316) having a mean ε^{54}Cr = 0.04 ± 0.07 (2SD, N = 6; Figure 1). The two aubrites with the extreme ε^{54}Cr values are Shallowater (-0.12 ± 0.04) and Khor Temiki (0.18 ± 0.04). Compared to aubrites, Itqiy and the enstatite achondrite clast in Almahatta Sitta, MS-MU-19, have lower ε^{54}Cr values, averaging at -0.26 ± 0.03 (2SD, N =2).

The mass-dependent Cr isotope data (δ^{53}Cr) for aubrites range from 0.10 ± 0.03 ‰ (Shallowater) to 0.30 ± 0.03 ‰ (Bustee), and bulk Itqiy possesses δ^{53}Cr of -0.03 ± 0.03 ‰. The relationship between the δ^{53}Cr and ε^{54}Cr values of these enstatite achondrites are shown in Figure 2a. Among main-group aubrites, δ^{53}Cr values broadly increase with bulk Mg# (Mg/(Mg+Fe)×100%, atom ratios; > 98; Figure 2b), but there is no correlation between their δ^{53}Cr values and bulk Cr contents (Figure 2c). The δ^{53}Cr values of main-group aubrites are, however, correlated with iron isotope compositions [expressed as δ^{56}Fe; (Wang et al., 2014)] (Figure 2d). Itqiy, Shallowater and main-group aubrites also have different and correlated Mg# and δ^{53}Cr values

303 (Figure 2b and Figure 3).

304 The measured ε^{53}Cr values range from 0.00 ± 0.02 for Shallowater up to 2.41 ±
305 0.03 for Bustee. Aside from these two samples and LAR 04316 (pieces) and
306 Cumberland Falls (small aliquot in this study), the ε^{53}Cr values of the remaining aubrite
307 samples, including those reported by Shukolyukov and Lugmair (2004), correlate with
308 their respective Mn/Cr ratios and form a ^{53}Mn-^{53}Cr correlation line with a slope of
309 0.225 ± 0.046 and an intercept of ε^{53}Cr of 0.50 ± 0.16 (MSWD = 9.8, N = 8; Figure 4a),
310 modeled by *Isoplot R* (Vermeesch, 2018), model 3 (MSWD >> 1). There is also a
311 correlation between ε^{53}Cr values and δ^{53}Cr values (Figure 4b).

312

4. Discussion

4.1 ε^{54}Cr systematics and the number of enstatite achondrite parent bodies

One of the complications for precise Cr isotope measurements of meteorites is their susceptibility to cosmic ray induced modifications. In aubrites, which are mostly composed of Fe-poor enstatite, this effect is negligible because iron is the primary target for producing Cr isotopes via cosmic ray exposure (Shima and Honda, 1966). Aubrites also have short cosmic ray exposure ages [up to 100 Ma; (Eugster, 2003; Lorenzetti et al., 2003)] compared to other meteorites such as mesosiderites which do not exhibit any cosmogenic effects on Cr isotopes themselves (Eugster, 2003; Trinquier et al., 2007). As such, modification of the Cr isotope systematics of aubrites by such processes is unlikely and not further considered.

The combination of ε^{54}Cr and Δ^{17}O signatures has been applied to investigate the kinship of Solar System materials (Trinquier et al., 2007; Warren, 2011; Zhu et al., 2021b). Most aubrites for which these data exist have indistinguishable ε^{54}Cr and Δ^{17}O values (Figure 1b), supporting the idea that the majority of aubrites originated from a single parent body. In addition, aubrites also have indistinguishable O and Cr isotopic composition with respect to the Earth, Moon and enstatite chondrites (Figure 1a), and similar ε^{54}Cr values but different Δ^{17}O values compared to R chondrites (Bischoff et al., 2011; Zhu et al., 2021a). Aside from the main aubrite population, some isotopically

distinct samples exist: Shallowater, a chondritic clast within Cumberland Falls, and Khor Temiki.

Although Shallowater has an indistinguishable $\Delta^{17}O$ value (-0.02 ± 0.02) from other aubrites (Newton et al., 2000), the $\varepsilon^{54}Cr$ value reported here is lower than the ones of other aubrites and enstatite chondrites, suggesting a distinct parent body. Formation of Shallowater from a distinct parent body is also consistent with its higher Fe and Cr content (Rubin, 2015; Watters and Prinz, 1979), heavier Zn and Fe isotope compositions (Moynier et al., 2011a; Wang et al., 2014), higher HSE contents (van Acken et al., 2012a) and more complex cooling history (Keil et al., 1989) relative to other aubrites.

The distinct and variable $\Delta^{17}O$ values reported for Cumberland Falls (Clayton et al., 1984; Miura et al., 2007; Newton et al., 2000) have been interpreted as representing the composition of ordinary chondrite-like clasts (Barrat et al., 2016; Verkouteren and Lipschutz, 1983) in this breccia. As such, the $\Delta^{17}O$ composition of Cumberland Falls cannot be taken as a robust genetic signature. Nonetheless, the sample of Cumberland Falls analyzed here has an indistinguishable $\varepsilon^{54}Cr$ value from other aubrites (with the exception of Shallowater) and enstatite chondrites. This value differs significantly from that of ordinary chondrites [-0.39 ± 0.09, 2SD; (Pedersen et al., 2019; Qin et al., 2010; Trinquier et al., 2007)] and, thus, suggests that the sample analyzed here is not compromised by the presence of ordinary chondrite material. Given its indistinguishable $\varepsilon^{54}Cr$ value with other aubrites, Cumberland Falls appears to belong

to the main group-aubrites. However, oxygen isotopes indicates that some limited isotopic heterogeneity existed within this meteorite.

The aubrite Khor Temiki, is characterized by a $\varepsilon^{54}Cr$ value of 0.18 ± 0.04 that is slightly higher but overlaps within uncertainties with some other aubrites, including Norton County (0.06 ± 0.09), LAR 04316 (0.06 ± 0.09) and Cumberland Falls (0.06 ± 0.09). Despite its slightly elevated $\varepsilon^{54}Cr$ value, Khor Temiki has an indistinguishable O isotope composition ($\Delta^{17}O = 0.01 \pm 0.02$) from other aubrites (Barrat et al., 2016) and lacks other evidence that could be used to distinguish it from other aubrites. As such, based on $\varepsilon^{54}Cr$ values, Khor Temiki may have originated from a distinct parent body than other aubrites or contain foreign, ^{54}Cr-rich clasts but additional data are required to test these hypotheses.

Itqiy ($\varepsilon^{54}Cr = -0.27 \pm 0.10$) and MS-MU-19 ($\varepsilon^{54}Cr = -0.25 \pm 0.08$) have the same $\varepsilon^{54}Cr$ values, consistent with their petrological similarities: they are both enstatite-rich, they lack plagioclase and are depleted in Na, K and V (Harries and Bischoff, 2020; Patzer et al., 2001). Although Itqiy has similar O isotope compositions as ECs and aubrites (Patzer et al., 2002), both Itqiy and MS-MU-19 show clearly different $\varepsilon^{54}Cr$ values from enstatite chondrites [0.03 ± 0.13; 2SD, N = 12; (Mougel et al., 2018; Qin et al., 2010; Trinquier et al., 2007)]. This observation suggests that they do not directly originate from enstatite chondrites and the aubrite (both main-group ones and Shallowater) parent bodies. The same $\varepsilon^{54}Cr$ values of Itqiy and MS-MU-19, and the similar petrology of Itqiy, NWA 2526, MS-MU-19 and MS-MU-36, supports that there

375 may be at least an additional enstatite-dominated asteroid (probably with a size of 500
376 km; Harries and Bischoff, 2020) in the Solar System, i.e. the Itqiy parent body. Thus,
377 combining petrological arguments with the ε^{54}Cr systematics allows us to distinguish at
378 least three isotopically distinct reservoirs that generated enstatite-rich achondrites: the
379 main-group aubrite parent body with $\varepsilon^{54}Cr = 0.06 \pm 0.12$ (2SD, N = 7), Shallowater
380 parent body with $\varepsilon^{54}Cr = -0.12 \pm 0.04$ and probably, the Itqiy parent body with $\varepsilon^{54}Cr =$
381 -0.26 ± 0.03 (2SD, N = 2). Note that this is not the same situation as for the ε^{54}Cr data
382 for monomict ureilites, which shows a broad compositional spectrum (i.e. continuous
383 variation, instead of showing three groups of enstatite achondrites), which is interpreted
384 as planetary mantle heterogeneity in a single parent body (Zhu et al., 2020b).

385 Hence, among the enstatite achondrites, only the ε^{54}Cr values of main-group
386 aubrites are indistinguishable from the Earth [(0.09 ± 0.12; 2SD, N = 17; (Mougel et al.,
387 2018; Trinquier et al., 2007)] and the Moon [(0.09 ± 0.08; (Mougel et al., 2018)], and
388 enstatite chondrites [0.02 ± 0.11; 2SD, N = 13; (Mougel et al., 2018; Qin et al., 2010;
389 Trinquier et al., 2007; Zhu et al., 2021b)] and most enstatite chondrite chondrules:
390 -0.11 ± 0.13 (2SD, N = 7) (Zhu et al., 2020a), which may indicate that they originated
391 from a common precursor reservoir. However, the main-group aubrites cannot directly
392 derive from enstatite chondrites, which will be further discussed in section 4.5. Finally,
393 the ε^{54}Cr sequence for non-carbonaceous achondrites (including the planets and
394 asteroids) can be updated as: Earth = Moon = main-group Aubrites > Shallowater >
395 Itqiy $\approx$ Mars > Angrites > Winonaites $\geqslant$ Acapulcoite-Lodranite Clan $\geqslant$ Vesta >

Ureilites (Li et al., 2018; Mougel et al., 2018; Qin et al., 2010; Trinquier et al., 2007; Yamakawa et al., 2010; Zhu et al., 2019b; Zhu et al., 2020b).

4.2 Chromium stable isotope fractionation during sulfide mineral crystallization

All aubrites and Itqiy (EH7-an; bulk) are enriched in the heavier isotopes of Cr with respect to chondrites and other differentiated parent bodies (Fig. 3). These distinct stable isotopic compositions must be the result of parent body processes since chondrites from different groups have homogeneous δ^{53}Cr values (Bonnand et al., 2016b; Schoenberg et al., 2016; Zhu et al., 2021a), which excludes Cr stable isotope fractionation by nebular processes. Chromium isotopes are fractionated during planetary processes, such as partial melting and fractional crystallization as observed for the Earth (Bonnand et al., 2020b; Schoenberg et al., 2008; Shen et al., 2019), the Moon (Bonnand et al., 2016a; Sossi et al., 2018) and Vesta (Zhu et al., 2019c). Moreover, equilibrium isotope fractionation by evaporation processes between oxidized vapor and reduced residue has been documented for lunar and Howardite-Eucrite-Diogenite (HED) samples (Sossi et al., 2018; Zhu et al., 2019c).

Aubrites are dominated by silicate minerals [≈ 99%, except for Shallowater; (Watters and Prinz, 1979)], predominantly enstatite and a minor plagioclase, diopside and forsterite. However, these silicate minerals are usually poor in Cr, mostly < ~300 ppm (Watters and Prinz, 1979). Chromium abundances in metals, i.e., kamacite and schreibersite, are even lower, ~20 ppm (Casanova et al., 1993). On the contrary, sulfide

417 minerals are usually rich in Cr, e.g., troilite, daubreelite, alabandite, caswellsilverite
418 and heideite can contain between ~0.5 (troilite) to ~37.4 (daubreelite) wt% Cr. The
419 much higher Cr content of sulfides relative to that of silicates and high silicate
420 abundance in main-group aubrites indicate that the bulk contents of Cr are controlled
421 primarily by silicate and sulfide minerals, since metal does not contribute much to the
422 Cr budget (Casanova et al., 1993). Therefore, the variations of the Cr contents and of
423 the δ^{53}Cr values possibly result from a two-endmember mixing between isotopically
424 heavy and Cr-poor silicates and isotopically light and Cr-rich sulfides. This is
425 consistent with *ab initio* calculations that predict that CrS and daubréelite ($FeCr_2S_4$) are
426 isotopically light compared to silicates (Moynier et al., 2011b). However, there is no
427 correlation between [δ^{53}Cr] and [1/Cr] (figure 2c) as would be expected for simple
428 mixing between sulfides (high Cr content and low δ^{53}Cr values) and silicates (low Cr
429 content and high δ^{53}Cr values). This could be due to secondary processes (i.e. an impact
430 event) that result in the equilibration of the Cr isotopes at the meteorite scale, while the
431 heterogeneous distribution of Cr-rich sulfide would significantly affect the Cr contents
432 of the different chips of a same meteorite. For example, Cumberland Falls shows
433 variable Cr contents, 945 ppm in this study and 549 ppm in Shukolyukov and Lugmair
434 (2004). Thus, it is difficult to determine the representative Cr contents (also the Mn/Cr
435 ratios) in bulk aubrite samples (i.e., different chips from one aubrite can have similar Cr
436 stable isotope compositions but distinct Cr contents), if the sample size is not large

enough, e.g., < 600 mg (Stracke et al., 2012). This sample heterogeneity effect is also discussed in section 4.4.

This two-endmember (silicate-sulfide) mixing for aubrites is reminiscent of the positive correlation between Fe content and Fe isotopes in aubrites (Wang et al., 2014). This has been interpreted as the mixing of isotopically light Fe from sulfide-rich metal with isotopically heavy, Fe-poor silicates (mantle material). In detail, Wang et al. (2014) argued the silicate in aubrites represent the mantle of aubrite parent body, while the metal is likely some residue in the mantle from incomplete metal-silicate differentiation (Casanova et al., 1993). A common origin for the δ^{53}Cr and δ^{56}Fe variability of aubrites, ignoring the anomalous Shallowater, is supported by their correlated variability (Figure 2d). However, because of its low Cr abundances, the Cr-poor Fe-Ni metal in aubrites (Casanova et al., 1993) cannot account for the Cr isotope variations. Instead, it is more likely that the variable presence of sulfide minerals (e.g., troilite) that are both rich in Fe and Cr (Keil, 2010a; Watters and Prinz, 1979) caused the observed correlated effects between Cr and Fe isotopes. This interpretation is also supported by experimental data that show equilibrium Fe isotope fractionation increases with sulfur content to ~0.4 ‰ at 18 wt.% sulfur in metal coexisting with silicate melt (Shahar et al., 2015).

4.3 Isotopically heavy Cr in the mantle of aubrite parent bodies induced by core formation

In order to use Cr stable isotopes to understand the formation and differentiation of the aubrite parent bodies (main-group and Shallowater), it is necessary to estimate

458 the $\delta^{53}Cr$ composition of their mantles. The depletion of HSE (van Acken et al., 2012a;
459 van Acken et al., 2012b) in aubrites compared to chondrites is evidence that their parent
460 body underwent core formation. However, given the high Cr content of sulfides
461 compared to silicates and their heterogeneous distribution within aubrites, obtaining a
462 pure silicate mantle composition requires a sulfide-free sample. Also, troilite, as the
463 major sulfide minerals in aubrites, contains Fe (~60%; (Watters and Prinz, 1979),
464 which given their chemical composition are usually interpreted as reflecting leftover
465 core material after incomplete core-mantle differentiation of the aubrite parent body
466 (Casanova et al., 1993). As explained above, Norton County has the highest Mg# (99.9)
467 and a bulk Cr content (180 ppm) comparable to the Cr content of typical silicate
468 minerals [<0.04%, (Keil, 2010a; Watters and Prinz, 1979)]. As such, the Cr isotope
469 composition of Norton County, $\delta^{53}Cr = 0.24 \pm 0.03$ ‰, is taken as the best estimation of
470 the mantle Cr isotope composition. Considering the silicate-sulfide mixing model for
471 Cr stable isotope variation, Bustee with heavier $\delta^{53}Cr$ value（0.30 ± 0.03 ‰) may also
472 indicate the silicate compositions and bulk silicate main-group aubrite parent body. The
473 elevated Cr contents and lower Mg# for Bustee can be also caused by sample
474 heterogeneity. However, the $\delta^{53}Cr$ values for both Norton County and Bustee are
475 resolvably heavier than those of chondrites, Shallowater and Itqiy. Given that
476 Shallowater and Itqiy are unique samples, their bulk $\delta^{53}Cr$ values of 0.10 ± 0.03 ‰ and
477 -0.03 ± 0.03 ‰ are our best approximation for their parent bodies' mantle. The mantle
478 $\delta^{53}Cr$ difference between the three parent bodies (Figure 3), consistent with their $\varepsilon^{54}Cr$

signatures (Figure 1b and 2a), confirms the existence of at least three enstatite achondrite parent bodies in the Solar System. This is also consistent with the difference in the mantle Mg# between three parent bodies (Figure 2b).

Chondrites have homogeneous Cr stable isotope compositions, with $\delta^{53}Cr = -0.12 \pm 0.04$ ‰ (2SD, N = 42) (Bonnand et al., 2016b; Schoenberg et al., 2016; Zhu et al., 2021a). The $\delta^{53}Cr$ values of all aubrites, including main-group, Shallowater and Itqiy are heavier than bulk chondrites as well as the mantles of other planetary bodies: Earth [-0.12 ± 0.04 ‰; (Jerram et al., 2020; Schoenberg et al., 2008; Sossi et al., 2018)], Moon [-0.21 ± 0.03 ‰; (Bonnand et al., 2016a; Sossi et al., 2018)] and Vesta [-0.22 ± 0.03 ‰; (Zhu et al., 2019c)] (Figure 3). These isotopic offsets: $\Delta_{\text{main-group aubrites-Chondrites}} = 0.36 \pm 0.05$ ‰, $\Delta_{\text{Shallowater-Chondrites}} = 0.22 \pm 0.05$ ‰ and $\Delta_{\text{Itqiy-Chondrites}} = 0.09 \pm 0.05$ ‰, combined with significant depletion in Cr between aubrites and chondrites (including enstatite chondrites) may provide significant insights into the origin of the bulk silicate aubrite parent bodies.

Several mechanisms may have caused the Cr stable isotope difference between chondrites and the bulk silicate aubrite parent bodies: 1) igneous processes, such as partial melting (e.g., Zhu et al., 2019c), 2) volatilization processes (e.g., Sossi et al., 2018; Zhu et al., 2019c) or 3) core formation (e.g., Bonnand et al., 2016b; Moynier et al., 2011b). Partial melting is a possible way to fractionate Cr stable isotopes, because of the potential exchange between "heavy" Cr^{3+} and "light" Cr^{2+} in residue and melts (e.g., Shen et al., 2019; Zhu et al., 2019c). This is also consistent with the fact that the

aubrites are depleted in basaltic components (Wilson and Keil, 1991). However, given the highly reduced conditions during aubrite differentiation (IW-2—IW-6), both the melt and residue are dominated by Cr^{2+} (Bell et al., 2020; Berry et al., 2006), and therefore partial melting is unlikely to fractionate Cr stable isotopes. Moreover, for the Earth's mantle, which is more oxidized than aubrites and contains both Cr^{2+} and Cr^{3+}, the extent of Cr isotopic fractionation is less than ~0.15 ‰ (based on the $\delta^{53}Cr$ difference between terrestrial chromite-free peridotites and chromites (Shen et al., 2015). This difference is much lower that what would be required to explain the difference between chondrites and main-group aubrite parent body (0.36 ± 0.05 ‰). Hence, partial melting cannot result in the observed Cr stable isotopic variations of the aubrites.

The volatility of Cr decreases together with fO_2, e.g., at fO_2 below IW = -2 and atmospheric pressure Cr becomes more refractory than Mg (Sossi et al., 2019). Thus, under reduced conditions volatile loss of Cr from aubrites should have resulted in concomitant losses of Mg which is not observed (Sedaghatpour and Teng, 2016). However, it is unknown whether the sulfur content affect the volatility of Cr, so we cannot totally exclude that the isotopically heavy Cr in aubrites is the result of evaporation (e.g., if sulfur increase the Cr volatility), considering that aubrite sulfides are rich in Cr (Watters and Prinz, 1979). Given the distinct Cr content and metal-sulfide abundance between bulk silicate aubrite parent body and ECs (Keil, 1968), and that Cr is not likely to be lost by volatilization, stable isotope fractionation

associated with core formation may be the most plausible mechanism to account for the heavier Cr in aubrites compared to chondrites.

The size of the aubrite parent body is not known, but is hypothesized to be probably <100 km based on models of the solubility of volatiles in basaltic melts of the aubrite parent body (Wilson and Keil, 1991). Chromium is mostly chalcophile, not siderophile, under the prevalent very low fO_2 of enstatite meteorites and low pressure conditions (Wood et al., 2008) and, thus, there should also be little Cr dissolved in the metallic core of the aubrite parent bodies. However, the partition coefficient of Cr into metal increases with the increasing sulfur content (Wood et al., 2014), which is also consistent with the high Cr content in the sulfide minerals in aubrites (Keil, 2010a; Watters and Prinz, 1979). Previous experiments have predicted that there should be very limited Cr stable isotope fractionation during metal-silicate segregation (Bonnand et al., 2016b). However, the experiments did not consider the composition effect of S, so it does not necessarily apply to aubrites, because the extremely reduced conditions during differentiation of aubrite parent body would likely form a core with abundant S. At present, it is difficult to provide a quantitative model to test the hypothesis that Cr isotope fractionation occurred during core formation. The core of the aubrite parent body may have contained both Fe-Ni-Si metal and sulfide. Unfortunately, even if the Cr contents in metal and sulfide were known, the proportions of metal and sulfide in the core cannot be estimated reliably, and thereby, the Cr contents in the core remain unknown.

The three enstatite achondrite parent bodies possess higher $\delta^{53}Cr$ values relative to other planets/asteroids, including Earth, Moon and Vesta (Figure 3). Earth possesses similar $\delta^{53}Cr$ values as chondrites (Bonnand et al., 2016b; Jerram et al., 2020; Schoenberg et al., 2016; Schoenberg et al., 2008; Sossi et al., 2018), suggesting that core formation did not fractionate Cr stable isotopes, which is consistent with the high temperature of Earth's core formation and further confirmed by high-pressure and high-temperature experiments (Bonnand et al., 2016b). Due to the relatively low temperature of the lunar core-mantle boundary (Cr is only siderophile at high temperature; (Corgne et al., 2008), only ~1% of the Moon's Cr would enter its core (Sossi et al., 2018). Therefore, the isotopically light Cr in lunar rocks is not due to core formation, but rather to a volatile loss during the magma ocean stage (Sossi et al., 2018). Also, Vesta, with a Cr-poor core, has lower $\delta^{53}Cr$ values than chondrites and enstatite achondrites, and its isotopically light Cr is interpreted to be caused by low-temperature volatile process rather than core formation (Zhu et al., 2019c). The Cr stable isotope composition of the Martian mantle is not well constrained, and in the future the physical conditions for the formation of the Martian core can be potentially traced with Cr isotopes.

4.4 Timescale of evolution of the main-group aubrite parent body

Aubrites are the product of magmatic differentiation on their parent body, which can potentially be dated using the ^{53}Mn-^{53}Cr chronometer (e.g., Shukolyukov and Lugmair, 2004). The $^{55}Mn/^{52}Cr$ ratio of Cumberland Falls reported by Shukolyukov

563 and Lugmair (2004), corresponding to 1.99, is different from the one determined here
564 (8.40). However, the two portions of Cumberland Falls have the same ε^{53}Cr values. A
565 similar observation has been made for leachates with variable ^{55}Mn/^{52}Cr ratios (0.04 –
566 9.58) for Bishopville (Shukolyukov and Lugmair, 2004) and two portions of LAR
567 04316 in this study, with ^{55}Mn/^{52}Cr ratios of 4.55 and 7.46, that all return similar ε^{53}Cr
568 values, suggesting that internal Mn/Cr redistribution post-dates ^{53}Mn decay and lack of
569 internal ^{53}Mn-^{53}Cr isochrons in aubrites. This situation does not mimic the leachates or
570 minerals (with variable ^{55}Mn/^{52}Cr ratios) in some individual angrites (Glavin et al.,
571 2004; Lugmair and Shukolyukov, 1998), eucrites (Lugmair and Shukolyukov, 1998)
572 and ureilites (Yamakawa et al., 2010), which show variable ε^{53}Cr values. Considering
573 the half-life of ^{53}Mn [(3.7 Myrs; (Holden, 1990)] combined with the Mn/Cr variability
574 in LAR 04316, Cumberland Falls and Bishopville and the precision of the ε^{53}Cr data,
575 the redistribution of Mn in these aubrites likely occurred after the extinction of ^{53}Mn,
576 i.e. >20 Myrs (eight half-life of ^{53}Mn; Figure 5) after Solar System formation.
577 Metamorphic redistribution of Mn and Cr on the meteorite scale might have occurred
578 by impact processes and is also supported by the fractionated trace elements and by
579 Ar-Ar ages (Biswas et al., 1980; Bogard et al., 2010). On the other hand, the
580 heterogeneous distribution of Mn/Cr ratios in aubrites, mainly caused by Mn- or
581 Cr-rich sulfide minerals, suggest that it will be difficult to determine the true ^{55}Mn/^{52}Cr
582 ratios of bulk aubrites. In other words, the ε^{53}Cr of each meteorite sample could be
583 representative of the bulk meteorite, while the ^{55}Mn/^{52}Cr ratio may not be, since

584 different sample fractions with variable Mn/Cr ratios have the same ε^{53}Cr values.

585 Aubrites do not all fall on the same line in a ε^{53}Cr against Mn/Cr ratio diagram
586 (Figure 4a), including the three data points from Shukolyukov and Lugmair (2004).
587 To limit nugget effects of Cr-rich sulfides in aubrites (that would result in a variation
588 of Mn/Cr ratios of bulk aubrites and would prohibit obtaining the "true" Mn/Cr ratios
589 of bulk aubrites), we focus on the largest samples that should be more representative
590 of the bulk sample composition. For this reason, we only consider the largest LAR
591 04316 sample (Table 1). Similarly, for Cumberland Falls, we use the data reported by
592 Shukolyukov and Lugmair (2004) (Cumberland Falls-SL; Table 1) that is obtained
593 from a large sample (905 mg) compared to ours (42 mg). Excluding also Bustee,
594 which has a very different Mn/Cr ratio in our study (1.42) compared to the literature
595 (6.08, Watters and Prinz, 1970) and Shallowater that is likely originating from a
596 different parent body, we obtain a correlation line (Figure 4a) for the main-group
597 aubrites. Using a model 3 (due to MSWD >> 1) regression of *Isoplot R*, this
598 ^{53}Mn-^{53}Cr correlation line for the main-group aubrites has an intercept (i.e., initial
599 ε^{53}Cr value) of 0.50 ± 0.16 and a slope of 0.225 ± 0.046 (MSWD = 9.8, N = 8). This
600 slope corresponding to a ^{53}Mn/^{55}Mn ratio of (2.55 ± 0.52) × 10^{-6}) can be translated to an
601 absolute date of 4562.5 ± 1.1 Ma, anchored to the U isotope corrected U-Pb age of
602 D'Orbigny angrite (Amelin, 2008; Brennecka and Wadhwa, 2012; Glavin et al., 2004).
603 This date is similar to that reported in Shukolyukov and Lugmair (2004), but in view of
604 our new stable isotope data, we interpret it was controlled by mixing of silicate and

605 sulfide minerals, and the time significance needs to be discussed.

606 Most aubrites are breccias (Keil, 2010a) and, as such, many are mixtures of rocks
607 with a different history. Hence, these rocks do not a have simple igneous history,
608 which limits the use of the ^{53}Mn-^{53}Cr system to obtain reliable age information such
609 as previously done for eucrites and diogenites (Trinquier et al., 2008b) and angrites
610 (Zhu et al., 2019b). This mixing history is also supported by the stable Cr isotope data
611 (section 3.2 and 3.3), suggesting that the δ^{53}Cr variation in aubrites is mainly
612 controlled by the relative abundance of sulfides and silicates. Finally, the δ^{53}Cr values
613 of aubrites positively correlate with their ε^{53}Cr values (Figure 4b). Their ε^{53}Cr values
614 mainly reflect the true ^{55}Mn/^{52}Cr ratios, because the Mn/Cr heterogeneity and
615 secondary processes for aubrites make it difficult to determine the representative
616 Mn/Cr ratios for bulk aubrite samples. This correlation indicates that the Cr in
617 aubrites are mixtures of Cr-rich sulfide (low Mn/Cr, low ε^{53}Cr and low δ^{53}Cr) and
618 Cr-poor silicates (high Mn/Cr, high ε^{53}Cr and high δ^{53}Cr).

619 Since aubrites are igneous rocks that experienced magmatic processes, both
620 silicate and sulfide should crystallize from the melt and derive from a common initial
621 reservoir. Considering this, the conditions for silicate and sulfide to define an isochron
622 are: 1) to be formed at the same time (crystallization from the same magma), 2) to
623 originate from the same reservoir (the melt) and 3) that possible later impact
624 metamorphism would not change the Mn/Cr ratios and Cr isotope compositions of the
625 bulk aubrites (closed system; but this could reset and flatted the internal isochron for

individual aubrites). In this respect, an external ^{53}Mn-^{53}Cr isochron age for main-group aubrites of 4562.5 ± 1.1 Ma would be valid and with time significance.

As suggested before for Mn-Cr whole rock isochrons of other planetary bodies (Lugmair and Shukolyukov, 1998; Trinquier et al., 2008b; Zhu et al., 2019b; Zhu et al., 2020b), the age from the bulk aubrite isochron likely records the timing of the differentiation of the main-group aubrite parent body, similar to those of Vesta, the angrite and ureilite parent bodies (Trinquier et al., 2008b; Zhu et al., 2019b; Zhu et al., 2020b). Mineral crystallization would also fractionate Mn/Cr ratios between aubrites. Enstatite in aubrites is typically characterized by low Mn and Cr contents (< 400 ppm for Mn and < 200 ppm for Cr) (Watters and Prinz, 1979). As such, the Mn/Cr fractionation between different main-group aubrites reflects variable incorporation of Mn-rich and Cr-rich minerals (e.g. oldhamite, daubreelite, caswellsilverite, heideite and niningerite) under reduced conditions during their crystallization. This age is very similar to the rock-forming age of Shallowater 4562.4 ± 0.2 Ma (Pravdivtseva et al., 2017), suggesting that the magmatic process for the enstatite achondrite parent bodies occurred at the same time. On the other hand, the differentiation time of the enstatite achondrite parent bodies is delayed compared to the ureilite parent body with ^{53}Mn-^{53}Cr age of 4566.7 ± 1.5 Ma (Zhu et al., 2020b), Vesta with ^{53}Mn-^{53}Cr age of 4564.8 ± 0.6 Ma (Trinquier et al., 2008b) and the angrite parent body with ^{53}Mn-^{53}Cr age of 4563.2 ± 0.3 Ma (Zhu et al., 2019b) when anchored to D'Orbigny.

4.5 The relationship between enstatite chondrites and aubrites and core formation based on the initial ε^{53}Cr values

The initial ε^{53}Cr value of the aubrite precursors defined by the intercept of the Mn-Cr isochron with the ordinate axis provides additional insight into the origin of aubrites and their potential genetic relationship to enstatite chondrites. The initial ε^{53}Cr value for the main-group aubrites (0.50 ± 0.16, 2σ) is significantly higher than the average ε^{53}Cr value of bulk enstatite (0.16 ± 0.06, 2SD, N = 12), Rumuruti (0.23 ± 0.05, 2SD, N = 12), carbonaceous (-0.04 ~ 0.27) and ordinary (0.19 ± 0.10, 2SD, N = 23) chondrites (Mougel et al., 2018; Qin et al., 2010; Trinquier et al., 2008b; Zhu et al., 2021a; Zhu et al., 2021b). This high initial ε^{53}Cr value is also consistent with the intercept of the three-point isochron from Shukolyukov and Lugmair (2004), but its implications have never been fully discussed. Moreover, whole-rock Mn-Cr isochrons for Vesta, angrite and ureilite parent bodies, which record Mn-Cr ages of ~2.5 Ma, ~4.1 Ma and ~0.5 Ma after CAIs, respectively, record lower initial ε^{53}Cr values than their parental melts of -0.12 ± 0.05 (Trinquier et al., 2008b), -0.10 ± 0.06 (Zhu et al., 2019b) and -0.24 ± 0.10 (Zhu et al., 2020b). It should also be noted that the initial ε^{53}Cr value of main-group aubrites is much higher than that of EC chondrules, -0.13 ± 0.07 (Zhu et al., 2020a), which are potential building blocks of enstatite achondrite parent bodies (e.g., Johansen et al., 2015). The higher initial ε^{53}Cr value as recorded by the aubrite whole rock isochron implies that the parent magma of the aubrites had a supra-chondritic Mn/Cr ratio. Shallowater is characterized by a low ε^{53}Cr value (0.00 ± 0.02) compared

667 to other aubrites, indicating that it evolved from another source with a resolvably lower
668 initial ε^{53}Cr value than those of the main-group aubrites. Combined with the ε^{54}Cr
669 systematics, the Cr isotope evidence strongly suggests that the main-group and
670 Shallowater aubrites should have distinct genetic origins.

671 The elevated initial ε^{53}Cr value of main-group aubrites compared to that of other
672 asteroids (e.g., Vesta, angrite and ureilite parent bodies) in the Solar System, indicates
673 that their parent melt had a high, non-chondritic, Mn/Cr ratio. A supra-chondritic
674 Mn/Cr ratio of the parent magma of main-group aubrite parent body can occur either if
675 the aubrite parent body precursor was characterized by a Mn/Cr ratio higher than
676 chondrites or if the Mn/Cr ratio of primitive melt for aubrites changed the during the
677 early evolution of the parent body. Note that the partition coefficient between FeS and
678 silicate melt, i.e. $D^{FeS/silicate\ melt}$, of Cr is higher than that of Mn (Berthet et al., 2009), so
679 the S-rich core formation process can efficiently increase the Mn/Cr ratio and ε^{53}Cr
680 value of the silicate melt of main-group aubrite parent body. This scenario is supported
681 by the S-rich core formation triggering large Cr stable isotope fractionation of aubrites
682 (see section 4.3). This is also consistent with that other S-poor and early formed rocky
683 planets, i.e. Vesta, angrite and ureilite parent body, have sub-chondritic initial ε^{53}Cr
684 values (Trinquier et al., 2008b; Zhu et al., 2019b; Zhu et al., 2020b).

685 Given the otherwise close kinship between aubrites and enstatite chondrites
686 expressed by their similarly reduced conditions, mineralogy and isotope compositions
687 (including Δ^{17}O, ε^{54}Cr and ε^{50}Ti values), it is more likely that the initial Mn/Cr ratio of

688 the aubrite parent body was close to chondritic. Therefore, aubrites may be the product
689 of post-core formation melting on an enstatite chondrite-like parent body that accreted
690 (Zhu et al., 2020a) and melted very early (e.g., < 2 Myr after Solar System formation) to
691 generate ^{53}Cr ingrowth prior to aubrite formation (Figure 5). Such early melting is
692 typically associated with large scale differentiation on other asteroids such as Vesta
693 (Schiller et al., 2011; Trinquier et al., 2008b) or the angrite parent body (Schiller et al.,
694 2015; Zhu et al., 2019b) due to the abundance of ^{26}Al at this time.
695

5. Conclusions

This work reported both the mass-independent and mass-dependent Cr isotope data for bulk enstatite achondrites, providing insights into the formation of their parent bodies in three ways, nucleosynthetic (ε^{54}Cr; origin), stable (δ^{53}Cr; process) and radiogenic (ε^{53}Cr; timing) isotope fractionations:

1. The ε^{54}Cr systematics define three groups of enstatite achondrites that likely represent three parent bodies, the main-group aubrite parent body with ε^{54}Cr of 0.06 ± 0.12 (2SD), Shallowater parent body with ε^{54}Cr = -0.12 ± 0.04 and Itqiy parent body with ε^{54}Cr = -0.26 ± 0.03 (2SD, N =2). This is consistent with their different δ^{53}Cr compositions: 0.24 ± 0.03 ‰, 0.10 ± 0.03 ‰ and -0.03 ± 0.03 ‰, respectively.

2. Mixing of different proportions of sulfides and silicates possibly result in the Cr stable isotope variation in aubrites. The globally heavy Cr in aubrites relative to that in chondrites could reflect large-scale Cr stable isotope equilibrium fractionation between sulfide (light) and silicate (heavy) followed by segregation of sulfide during core formation, resulting in isotopically heavy mantle.

3. The aubrite samples record heterogeneous distribution of Mn and Cr. The ^{53}Mn-^{53}Cr correlation for the main-group aubrites (except Bustee) is a mixing line but also an isochron that holds a time significance of the crystallization of silicate and sulfide minerals and return an absolute age of 4562.5 ± 1.1 Ma (i.e. 4.8 ± 1.1 Ma after CAIs). This most likely represents the age of the silicate differentiation on the

716 main-group aubrite body. The absence of internal Mn-Cr isochrons for individual
717 aubrites implies that they underwent metamorphic redistribution of Mn and Cr after
718 ^{53}Mn extinction, maybe following a disruption event of the parent body.

719 4. The initial ε^{53}Cr value for main-group aubrites are higher than the ε^{53}Cr values
720 for enstatite chondrites, suggesting the main-group aubrites did not directly originate
721 from enstatite chondrites. Instead, the high initial ε^{53}Cr values of main-group aubrites
722 are potentially caused by an early sulfur-rich core formation that efficiently increased
723 the Mn/Cr ratio of the silicate fraction.
724

Acknowledgements

Constructive comments from Jan Render, Royji Tanaka and Rick Carlson greatly improved this manuscript, and comments and editorial handling from the associate editor Yves Marrocchi are also appreciated. F. M. acknowledges funding from the European Research Council under the H2020 framework program/ERC Starting Grant Agreement (#637503–PRISTINE) and financial support of the UnivEarthS Labex program at Sorbonne Paris Cité (#ANR–10–LABX–0023 and #ANR–11–IDEX-0005-02), and the ANR through a chaire d'excellence Sorbonne Paris Cité. M. B. acknowledges funding the Carlsberg Foundation (CF18-1105), the Danish National Research Foundation (DNRF97) and the European Research Council (ERC Advanced Grant Agreement, #833275–DEEPTIME). M. S. acknowledges funding from the Villum Fonden (#00025333). Parts of this work were supported by IPGP multidisciplinary program PARI, and by Paris–IdF region SESAME (#12015908). Pierre Burckel and Pascale Louvat were appreciated for analysis on ICP-MS and MC-ICP-MS at IPGP, respectively. We thank Ninja Braukmüller, Monika Feth, Maren Saenz, Elis Hoffmann and Yogita Kadlag for technical support at FUB. Discussions with Paolo Sossi about Cr stable isotope fractionation in S-rich core formation helped us interpret the data. K. Z. thanks an Alexander von Humboldt fellowship (for postdoc researchers), China Scholarship Council (CSC) for a PhD fellowship (#201706340161) and a TRR 170 fellowship during his stay in Berlin in autumn 2020. H.B. is funded by

745 the Deutsche Forschungsgemeinschaft (DFG, German Research Foundation–
746 #263649064–TRR 170). This is TRR 170 publication no. 135.
747

Appendix

Individual data for TIMS total-evaporation measurements

Sample	Itqiy		MS-MU-19		Allende		DTS-1	
N	$\varepsilon^{53}Cr$	$\varepsilon^{54}Cr$	$\varepsilon^{53}Cr$	$\varepsilon^{54}Cr$	$\varepsilon^{53}Cr$	$\varepsilon^{54}Cr$	$\varepsilon^{53}Cr$	$\varepsilon^{54}Cr$
1	0.50	-0.33	1.87	-0.15	0.19	1.01	0.19	0.31
2	0.56	0.06	1.78	-0.26	0.11	0.75	0.11	0.30
3	0.60	-0.23	1.78	-0.10	0.11	0.90	0.05	0.18
4	0.48	-0.55	1.71	-0.50	-0.04	0.67	0.05	0.41
5	0.44	-0.59	1.87	-0.29	0.12	1.01	-0.04	0.05
6	0.55	-0.22	1.65	-0.45	0.08	0.82	-0.01	0.08
7	0.43	-0.44	1.76	-0.33	0.05	0.84	-0.01	0.10
8	0.65	-0.20	1.72	-0.11	0.02	0.72	0.05	0.22
9	0.55	-0.16	1.77	-0.29	0.03	0.85	-0.10	-0.11
10	0.59	-0.17	1.66	-0.15	0.01	0.55	0.11	0.28
11	0.52	-0.07	1.80	-0.15			-0.04	0.01
12	0.46	-0.32					0.00	0.01
13	0.50	-0.21						
14								
Average	**0.52**	**-0.27**	**1.76**	**-0.25**	**0.07**	**0.81**	**0.03**	**0.15**
2SD	0.13	0.37	0.14	0.27	0.13	0.29	0.16	0.31
2SE	0.04	0.10	0.04	0.08	0.04	0.09	0.05	0.09

Table 1 Cr (both mass-independent and mass-dependent) and O isotopes data for aubrites.

Name	Fall/Find	Texture/Type	Mass (mg)	Cr content (ppm)	Mg#	Fe/Cr	$^{55}Mn/^{52}Cr$	$\varepsilon^{53}Cr$	2SE	$\varepsilon^{54}Cr$	2SE	N/Ref.	$\Delta^{17}O$	Error	Ref.	$\delta^{53}Cr$	2SD	N
Khor Temiki	Fall	Fragmental breccia	39.8	742	98.8	14.6	3.77	**1.39**	0.01	**0.18**	0.04	5	0.01	0.02	[2]	**0.22**	0.03	2
Bustee	Fall	Regolith breccia	33.7	2221	99.1	3.5	1.42	**2.41**	0.03	**0.02**	0.06	5	0.01	0.00	[2]	**0.30**	0.03	2
Norton County	Fall	Fragmental breccia	40.0	180	99.9	6.5	4.37	**1.53**	0.06	**0.06**	0.09	5	0.01	0.01	[2]	**0.24**	0.03	1
ALH 78113	Find	Fragmental breccia	43.5	1439	98.1	11.9	2.58	**0.97**	0.02	**-0.03**	0.06	5	0.09	0.02	[3]	**0.12**	0.03	2
ALH 84007	Find	Fragmental breccia	50.7	758	99.2	9.1	2.34	**1.08**	0.01	**0.06**	0.04	5	0.05	0.03	[3]	**0.23**	0.03	2
LAR 04316 (powder)	Find	Fragmental breccia	46.0	1109	98.7	10.0	4.55	**1.48**	0.02	**0.06**	0.09	5	0.04	0.01	[2]	**0.23**	0.03	2
LAR 04316 (pieces)			26.4	861	98.7	13.1	7.46	**1.49**	0.00*	**0.06**	0.05	5				**0.16**	0.03	2
Shallowater	Find	Unbrecciated	30.9	4597	77.7	42.2	0.33	**0.00**	0.02	**-0.12**	0.04	5	-0.02	0.02	[3]	**0.10**	0.03	2
Peña Blanca Spring	Fall	Fragmental breccia	898	394			3.01	**1.16**	0.05			15/[1]	0.01	0.01	[2]			
Bishopville	Fall	Fragmental breccia	911	273			3.79	**1.34**	0.08			17/[1]	-0.05	0.06	[3]			
Cumberland Falls	Fall	Fragmental breccia	42.0	945	98.2	17.2	8.40	**1.11**	0.05	**0.06**	0.09	5	0.15	0.55	[3,4,5]	**0.19**	0.03	2
Cumberland Falls-SL			905	549			1.99	**1.00**	0.09			14/[1]						
Chondritic Clast in Cumberland Falls		Clast											0.65	0.02	[2]			
Itqiy#	Find	Unbrecciated-EH7		830	65.1	25.7		**0.52**	0.04	**-0.27**	0.10	13	0.06	0.08	[6]	**-0.03**	0.03	3
MS-MU-19#	Fall	Clast						**1.76**	0.04	**-0.25**	0.08	11						
Allende#	Fall	CV chondrite						**0.07**	0.04	**0.81**	0.09	10						
DTS-1#		Terrestrial dunite						**0.03**	0.05	**0.15**	0.09	12						

Note: References: [1] (Shukolyukov and Lugmair, 2004), [2] (Barrat et al., 2016), [3] (Newton et al., 2000), [4] (Clayton et al., 1984), [5] (Miura et al., 2007) and [6] (Patzer et al., 2002). The $\delta^{53}Cr$ and elemental data for Itqiy are from a bulk sample, while the $\varepsilon^{53}Cr$ and $\varepsilon^{54}Cr$ data for Itqiy and MS-MU-19 are from leached

samples with mostly silicate (the metal and sulfide were removed the by HCl). The Cr content, Mg# (Mg/(Mg+Fe)×100%, atom ratios) and Fe/Cr (atom ratios) are measured by ICP-MS, with an error of 5-10% (2se), except for the data for bulk Itqiy that are from (Patzer et al., 2001). N is then number of runs. The data marked * indicates the 2SE uncertainty is less than 0.004. The data for sample marked # are measured by total evaporation method on Triton TIMS housed at Freie Universität Berlin.

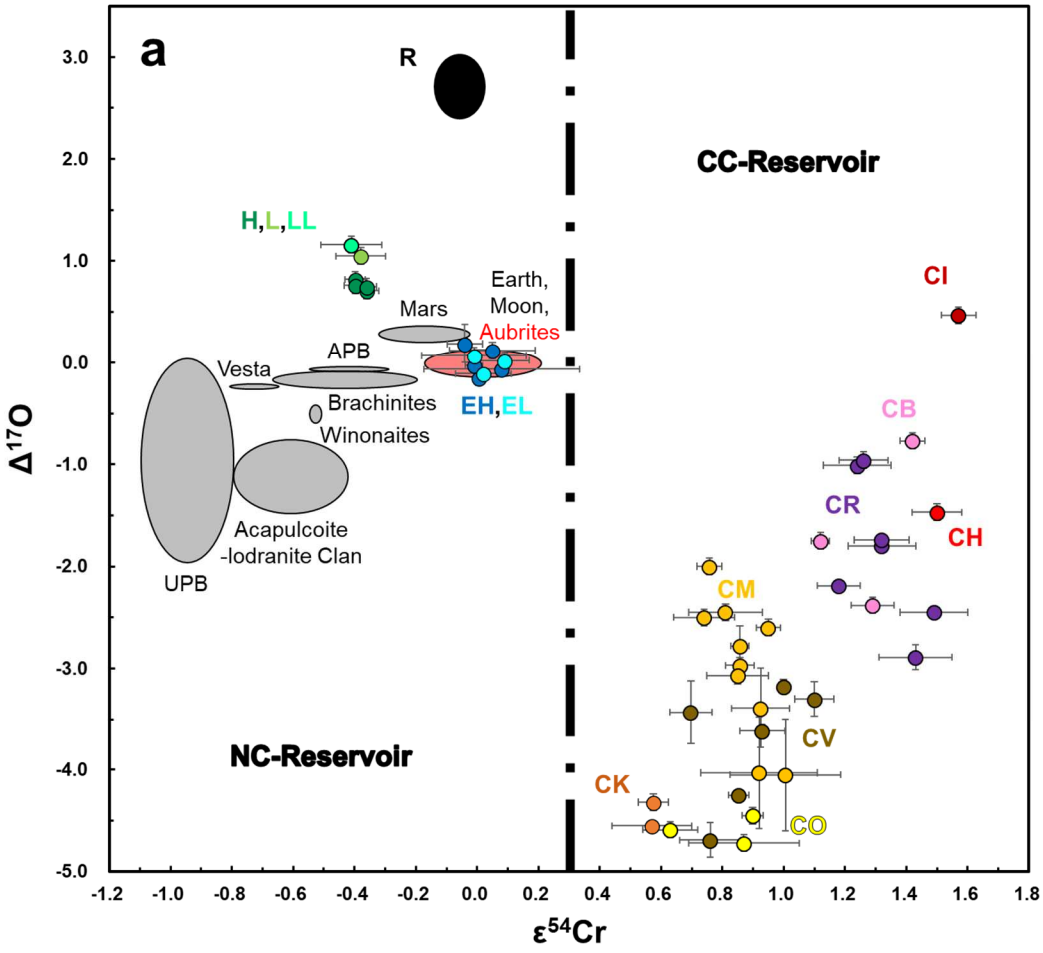
a
R
CC-Reservoir
NC-Reservoir
H,L,LL
Earth,
Moon,
Aubrites
Mars
APB
Vesta
Brachinites
Winonaites
EH,EL
Acapulcoite
-lodranite Clan
UPB
CI
CB
CR
CH
CM
CV
CK
CO
Δ17O
ε54Cr

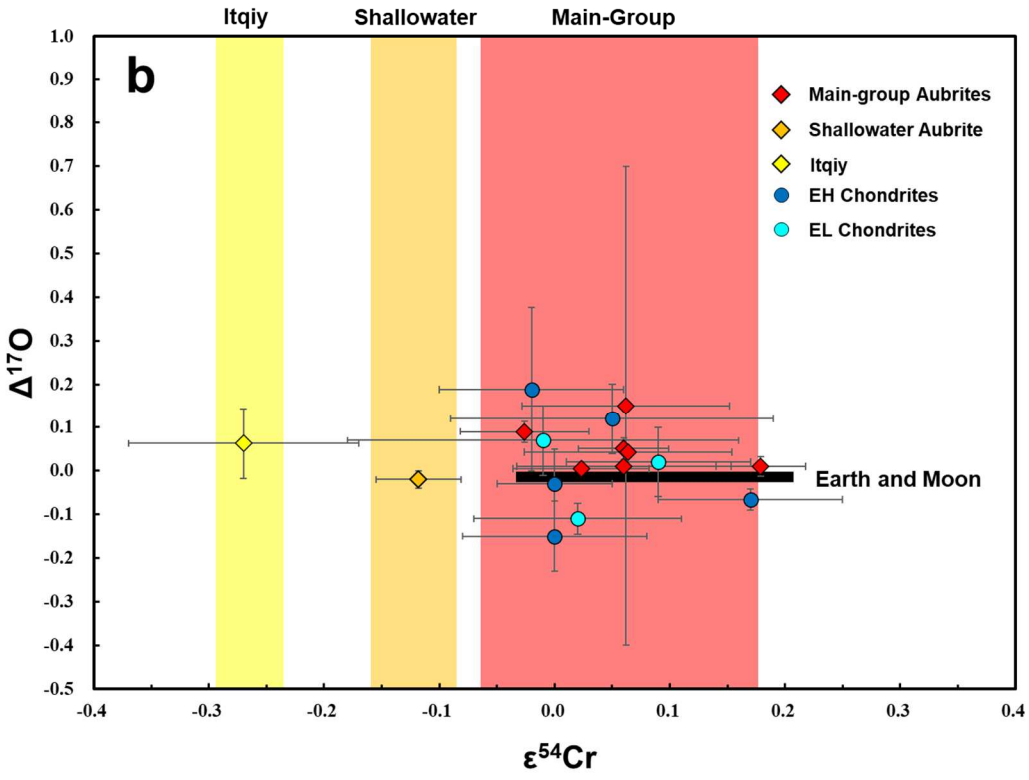
Itqiy
Shallowater
Main-Group
b
Main-group Aubrites
Shallowater Aubrite
Itqiy
EH Chondrites
EL Chondrites
Earth and Moon
Δ17O
ε54Cr

1

Figure 1a. The $\varepsilon^{54}Cr$ - $\Delta^{17}O$ diagram for aubrites, enstatite chondrites and other Solar System materials. The area of enstatite meteorites (in red) overlaps with that of Earth-Moon system. The template and dataset (all the data cited are from published literature and no conference abstracts) are from Zhu et al. (2021b), and the data sources are mainly from Schiller et al. (2014), Trinquier et al. (2007), Yamashita et al. (2010), Qin et al. (2010), Göpel et al. (2015), Pedersen et al. (2019), Mougel et al. (2018), Clayton and Mayeda (1999), Clayton and Mayeda (1984), Greenwood et al. (2010), Clayton et al. (1991), Clayton et al. (1984), Greenwood et al. (2017), Newton et al. (2000), Schrader et al. (2011), Petitat et al. (2011), Zhu et al. (2020b), Zhu et al. (2020a), Zhu et al. (2019b), Li et al. (2018), Zhu et al. (2020b), Yamakawa et al. (2010), Greenwood et al. (2017), Zhu et al. (2020b), Ireland et al. (2020), Zhu et al. (2021a) and Bischoff et al. (2011). The colored circles are chondrites, while the grey shade areas indicate planets/asteroids (i.e., achondrite parent bodies). **Figure 1b.** The zoomed figure for the aubrite area of figure 1a. The enstatite achondrites are diamonds, and the error for $\varepsilon^{54}Cr$ data are reported as the 2SE, while the error for grouping $\varepsilon^{54}Cr$ (shades) of main-group aubrites and Itqiy is the 2SD. The $\varepsilon^{54}Cr$ and $\Delta^{17}O$ for main-group aubrites overlap those the enstatite chondrite and Earth-Moon system (black bar), but Shallowater has a different $\varepsilon^{54}Cr$ value compared to other aubrites, enstatite chondrites and Earth-Moon system. The red-orange-yellow shades indicate the three enstatite achondrite parent bodies inferred from $\varepsilon^{54}Cr$ systematics.

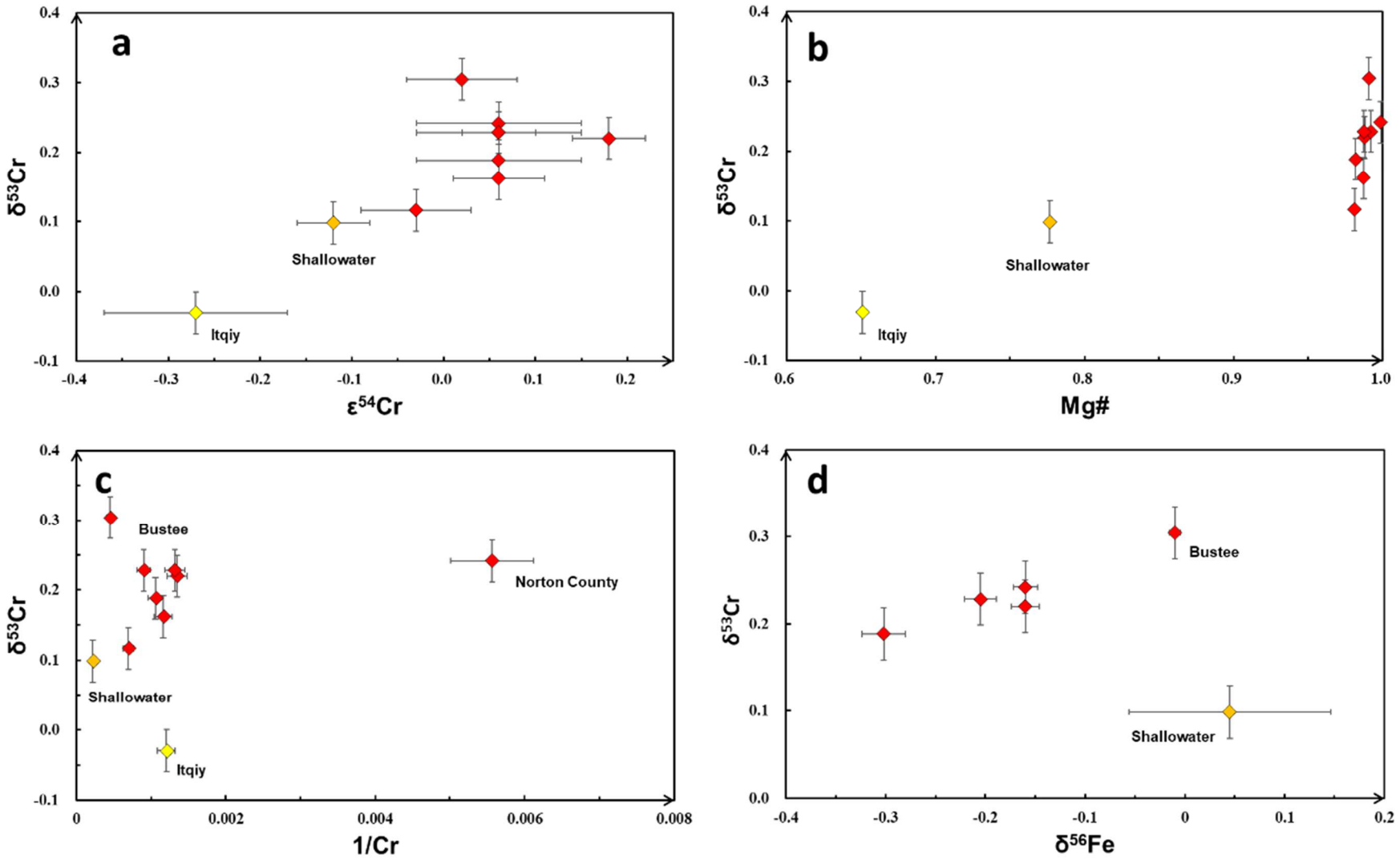
a
b
c
d
δ53Cr
ε54Cr
Mg#
1/Cr
δ56Fe
Shallowater
Itqiy
Bustee
Norton County

21

Figure 2a. $\varepsilon^{54}Cr$-$\delta^{53}Cr$ values for enstatite achondrites, with the red diamonds for main-group aubrites, the orange diamond for Shallowater and the yellow diamond for Itqiy. There is no correlation between $\varepsilon^{54}Cr$ and $\delta^{53}Cr$ values of main-group aubrites, suggesting the mass-independent data are not influenced by the mass-dependent fractionation. The different $\delta^{53}Cr$ values between the three groups of enstatite achondrites suggests they formed from different processes, which is consistent with their different $\varepsilon^{54}Cr$ values suggesting at least three enstatite chondrite parent bodies. **Figure 2b**. Mg#-$\delta^{53}Cr$ values for aubrites. Except Shallowater and Itqiy, all main-group aubrites have high Mg# (98-100%). The three enstatite achondrite parent bodies have correlated Mg# and $\delta^{53}Cr$ values. **Figure 2c.** 1/Cr-$\delta^{53}Cr$ values of aubrites. The uncertainty of Cr contents is estimated as 5% (2σ). There is no correlation between 1/Cr and $\delta^{53}Cr$. The reason for the lack of mixing correlation here could be the sample heterogeneity and secondary processes (most likely impact). **Figure 2d.** $\delta^{56}Fe$-$\delta^{53}Cr$ values for aubrites. The $\delta^{56}Fe$ isotope data are from Wang et al., (2011), and the data with multiple measurements are averaged with 2SD uncertainty. The correlation between $\delta^{56}Fe$ and $\delta^{53}Cr$ values for main-group aubrites should reflect a mixing between sulfide-metal and silicates. The sulfide-metal are rich in both isotopically light Cr and Fe, while the silicates possess isotopically heavy Cr and Fe.

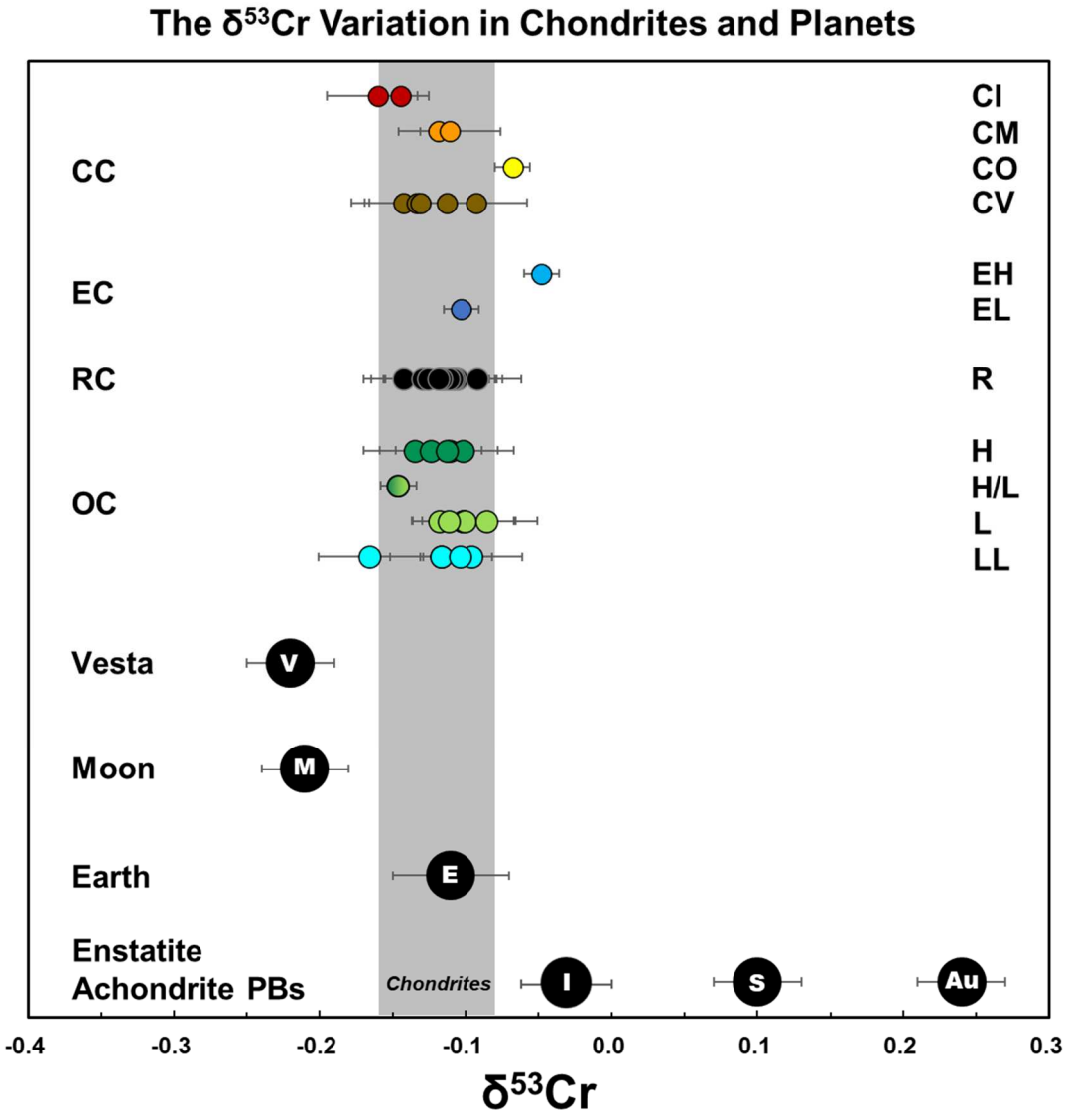

Figure 3. Comparison of the $\delta^{53}Cr$ variations amongst chondrites, achondrites and the Earth-Moon system. The small colorful circles are chondrites, while the big black circles represent the Earth, Moon, Vesta and enstatite achondrite parent bodies. The gray bar defines the average $\delta^{53}Cr$ values (-0.12 ± 0.04; 2SD, N =42) of all the chondrites, and the three enstatite achondrite parent bodies have distinguished mass-dependent Cr isotope compositions ($\delta^{53}Cr$ values): 0.24 ± 0.03 ‰, 0.10 ± 0.03 ‰ and -0.03 ± 0.03 ‰ for main-group aubrite (Au), Shallowater (S) and Itqiy (I) parent bodies respectively, which is consistent their $\varepsilon^{54}Cr$ characteristics. The $\delta^{53}Cr$ difference between enstatite achondrite parent bodies and chondrites result from a sulfur-rich core formation. Itqiy and Shallowater parent bodies have lower $\delta^{53}Cr$ values than main-group aubrites, which may result from more sulfides-metal contents (lower Mg#) in Shallowater and Itqiy. This is consistent with the mixing models in figure 2d. Literature data sources: chondrites (Bonnand et al., 2016b; Schoenberg et al., 2016), Earth (Jerram et al., 2020; Schoenberg et al., 2008; Sossi et al., 2018), Moon (Bonnand et al., 2016a; Sossi et al., 2018) and HEDs-Vesta (Zhu et al., 2019c).

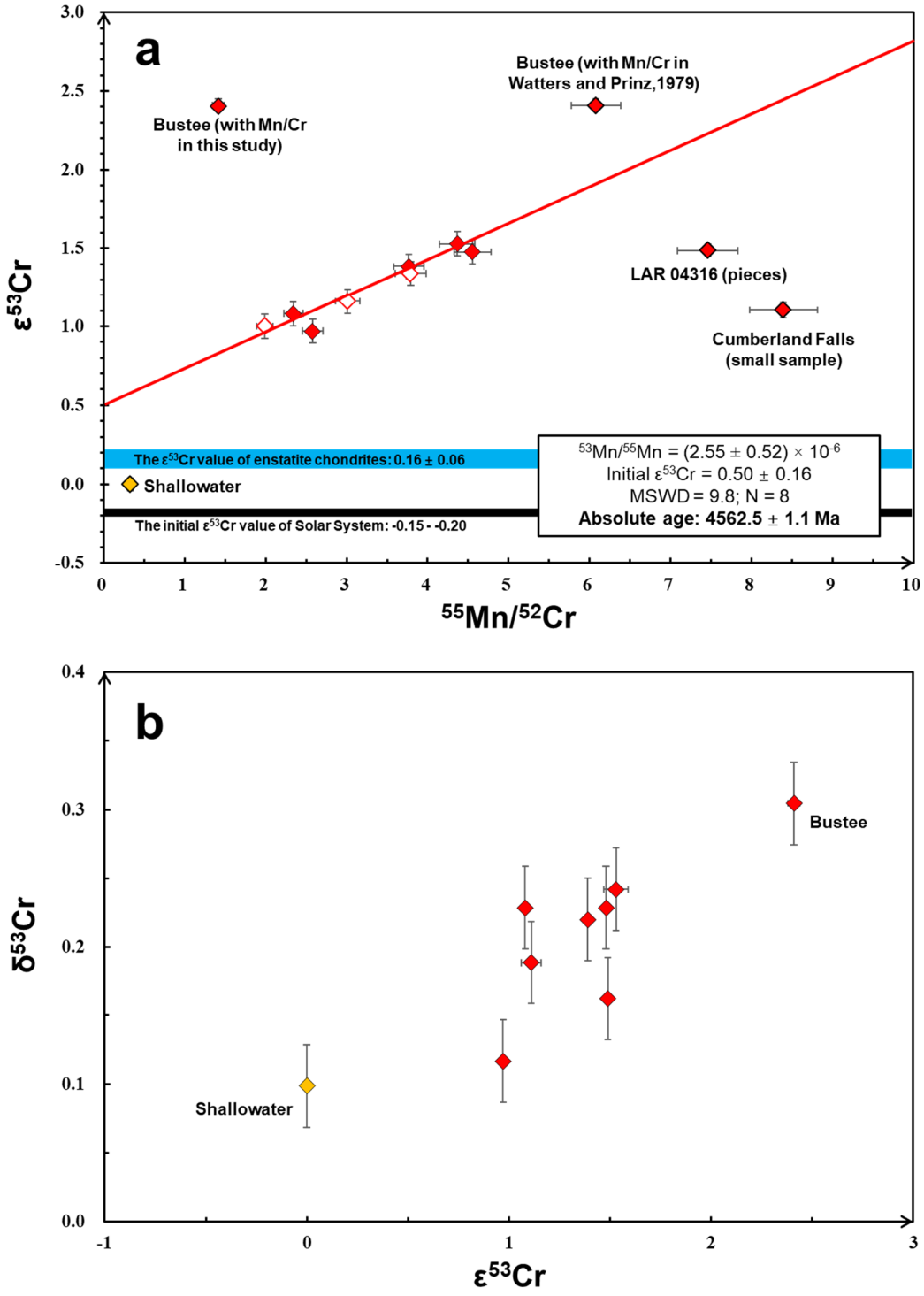

Figure 4a. The ^{53}Mn-^{53}Cr isochron for bulk aubrites, the open diamonds are the Cr isotope data from Shukolyukov and Lugmair (2004). This red correlation line does not include Shallowater, Bustee, LAR 04316 (pieces) and Cumberland Falls (small sample) from this study, due to the different parent bodies and sample heterogeneity. The blue and black bars are the ε^{53}Cr value of enstatite chondrites and the initial ε^{53}Cr value of Solar System that is estimated by D'Orbigny angrite, CI chondrite and chondrule precursors (Göpel et al., 2015; Trinquier et

al., 2008b; Zhu et al., 2019a). The ^{53}Mn-^{53}Cr correlation line is controlled by co-genetic sulfide and silicates, which also holds the time significance reflecting the differentiation of main-group parent body and crystallization of sulfide and silicates. More importantly, the elevated initial $\varepsilon^{53}Cr$ value (0.50 ± 0.16, 2σ; higher than that of the Solar System and enstatite chondrites), expressed by the intercept of y axis, could be caused by the early S-rich core formation process. **Figure 4b.** The $\delta^{53}Cr$ values correlate with the $\varepsilon^{53}Cr$ values that mainly reflect the true Mn/Cr ratios (since there is a large Mn/Cr heterogeneity in aubrites). This correlation indicates that the aubrites reflect mixing of lithologies with more abundant Cr-rich sulfide (low Mn/Cr, low $\varepsilon^{53}Cr$ and low $\delta^{53}Cr$) and lithologies with Cr-poor silicates (high Mn/Cr, high $\varepsilon^{53}Cr$ and high $\delta^{53}Cr$).

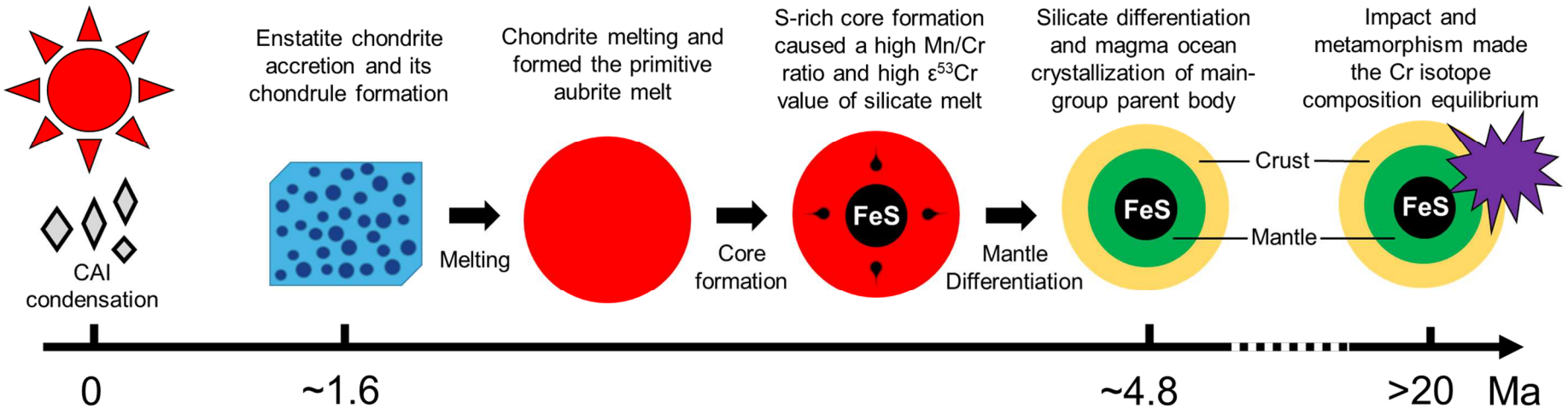

Figure 5 The timeline of evolution of the main-group aubrite parent body. The Ca-Al-rich inclusion condensation marked the formation of the Solar System (t_0, 4567.30 ± 0.16 Ma) (Connelly et al., 2012). Then, enstatite chondrite chondrules formed at 4565.7 ± 0.7 Ma (precursor age), i.e. ~1.6 Ma after t_0 (Zhu et al., 2020a), and the accretion of enstatite chondrites is estimated as ~1.8 Ma after t_0 (Alexander et al., 2018). These two ages can potentially represent the accretion time of enstatite chondrites. After that, enstatite chondrites experienced a melting event and formed the primitive aubrite melt. At this stage, this melt has chondritic Mn/Cr ratio. Then, the sulfur-rich core formation process changed the composition of the primitive melt, making the core rich in Cr and poor in Mn (Berthet et al., 2009), while the silicate melt possessing high Mn/Cr ratio. In this way, after the decay of ^{53}Mn, the silicate melt has a high ε^{53}Cr value that is the source of main-group aubrites. It furthermore experienced a silicate differentiation and mineral crystallization that fractionates the Mn/Cr ratios in main-group aubrites. The ^{53}Mn-^{53}Cr system recorded the age of this event, 4562.5 ± 1.1 Ma (i.e. 4.8 ± 1.1 Ma after CAIs), which indicates the differentiation time of main-group aubrite parent body. Finally, after extinction of ^{53}Mn (around eight times of the half-life of ^{53}Mn) , i.e. ~20 Ma after t_0, there should be a metamorphosed process, mostly caused by impact, redistributed the Mn and Cr in individual aubrites and reset the internal ^{53}Mn-^{53}Cr isochrons.

References

Alexander, C.M.D., McKeegan, K.D. and Altwegg, K. (2018) Water reservoirs in small planetary bodies: meteorites, asteroids, and comets. Space Science Reviews 214, 36.

Amelin, Y. (2008) U–Pb ages of angrites. Geochimica et Cosmochimica Acta 72, 221-232.

Baker, J.A., Schiller, M. and Bizzarro, M. (2012) ^{26}Al–^{26}Mg deficit dating ultramafic meteorites and silicate planetesimal differentiation in the early Solar System? Geochimica et Cosmochimica Acta 77, 415-431.

Barrat, J., Greenwood, R., Keil, K., Rouget, M., Boesenberg, J., Zanda, B. and Franchi, I. (2016) The origin of aubrites: Evidence from lithophile trace element abundances and oxygen isotope compositions. Geochimica et Cosmochimica Acta 192, 29-48.

Bell, A.S., Vaci, Z. and Lanzirotti, A. (2020) An Experimental-XANES Investigation of the Cr Valence Systematics in Basaltic Liquids and Applications to Modeling Cr2+/ΣCr Evolution in Crystallizing Basaltic Magma Systems. Geochimica et Cosmochimica Acta.

Berry, A.J., O'Neill, H.S.C., Scott, D.R., Foran, G.J. and Shelley, J. (2006) The effect of composition on Cr2+/Cr3+ in silicate melts. American Mineralogist 91, 1901-1908.

Berthet, S., Malavergne, V. and Righter, K. (2009) Melting of the Indarch meteorite (EH4 chondrite) at 1 GPa and variable oxygen fugacity: Implications for early planetary differentiation processes. Geochimica et Cosmochimica Acta 73, 6402-6420.

Birck, J.-L. and Allègre, C.J. (1988) Manganese—chromium isotope systematics and the development of the early Solar System. Nature 331, 579-584.

Bischoff, A., Vogel, N. and Roszjar, J. (2011) The Rumuruti chondrite group. Geochemistry 71, 101-133.

Biswas, S., Walsh, T., Bart, G. and Lipschutz, M.E. (1980) Thermal metamorphism of primitive meteorites—XL The enstatite meteorites: origin and evolution of a parent body. Geochimica et Cosmochimica Acta 44, 2097-2110.

Bizzarro, M., Paton, C., Larsen, K., Schiller, M., Trinquier, A. and Ulfbeck, D. (2011) High-precision Mg-isotope measurements of terrestrial and extraterrestrial material by HR-MC-ICPMS—implications for the relative and absolute Mg-isotope composition of the bulk silicate Earth. Journal of Analytical Atomic Spectrometry 26, 565-577.

Bogard, D.D., Dixon, E.T. and Garrison, D.H. (2010) Ar-Ar ages and thermal histories of enstatite meteorites. Meteoritics & Planetary Science 45, 723-742.

Bonnand, P., Bruand, E., Matzen, A.K., Jerram, M., Schiavi, F., Wood, B.J., Boyet, M. and Halliday, A.N. (2020a) Redox control on chromium isotope behaviour in silicate melts in contact with magnesiochromite. Geochimica et Cosmochimica Acta 288, 282-300.

Bonnand, P., Doucelance, R., Boyet, M., Bachèlery, P., Bosq, C., Auclair, D. and Schiano, P. (2020b) The influence of igneous processes on the chromium isotopic

115 compositions of Ocean Island basalts. Earth and Planetary Science Letters 532, 116028.
116 Bonnand, P., Parkinson, I.J. and Anand, M. (2016a) Mass dependent fractionation of
117 stable chromium isotopes in mare basalts: Implications for the formation and the
118 differentiation of the Moon. Geochimica et Cosmochimica Acta 175, 208-221.
119 Bonnand, P., Williams, H.M., Parkinson, I.J., Wood, B.J. and Halliday, A.N. (2016b)
120 Stable chromium isotopic composition of meteorites and metal–silicate experiments:
121 Implications for fractionation during core formation. Earth and Planetary Science
122 Letters 435, 14-21.
123 Brennecka, G.A. and Wadhwa, M. (2012) Uranium isotope compositions of the basaltic
124 angrite meteorites and the chronological implications for the early Solar System.
125 Proceedings of the National Academy of Sciences 109, 9299-9303.
126 Casanova, I., Keil, K. and Newsom, H.E. (1993) Composition of metal in aubrites:
127 Constraints on core formation. Geochimica et Cosmochimica Acta 57, 675-682.
128 Clayton, R.N. and Mayeda, T.K. (1984) The oxygen isotope record in Murchison and
129 other carbonaceous chondrites. Earth and Planetary Science Letters 67, 151-161.
130 Clayton, R.N. and Mayeda, T.K. (1999) Oxygen isotope studies of carbonaceous
131 chondrites. Geochimica et Cosmochimica Acta 63, 2089-2104.
132 Clayton, R.N., Mayeda, T.K., Goswami, J. and Olsen, E.J. (1991) Oxygen isotope
133 studies of ordinary chondrites. Geochimica et Cosmochimica Acta 55, 2317-2337.
134 Clayton, R.N., Mayeda, T.K. and Rubin, A.E. (1984) Oxygen isotopic compositions of
135 enstatite chondrites and aubrites. Journal of Geophysical Research: Solid Earth 89,
136 C245-C249.
137 Connelly, J.N., Bizzarro, M., Krot, A.N., Nordlund, Å., Wielandt, D. and Ivanova, M.A.
138 (2012) The absolute chronology and thermal processing of solids in the solar
139 protoplanetary disk. Science 338, 651-655.
140 Corgne, A., Keshav, S., Wood, B.J., McDonough, W.F. and Fei, Y. (2008) Metal–
141 silicate partitioning and constraints on core composition and oxygen fugacity during
142 Earth accretion. Geochimica et Cosmochimica Acta 72, 574-589.
143 Ebel, D.S. and Alexander, C.M.O.D. (2011) Equilibrium condensation from chondritic
144 porous IDP enriched vapor: Implications for Mercury and enstatite chondrite origins.
145 Planetary and Space Science 59, 1888-1894.
146 Eugster, O. (2003) Cosmic-ray Exposure Ages of Meteorites and Lunar Rocks and
147 Their Significance. Geochemistry 63, 3-30.
148 Glavin, D., Kubny, A., Jagoutz, E. and Lugmair, G. (2004) Mn-Cr isotope systematics
149 of the D'Orbigny angrite. Meteoritics & Planetary Science 39, 693-700.
150 Göpel, C., Birck, J.-L., Galy, A., Barrat, J.-A. and Zanda, B. (2015) Mn–Cr systematics
151 in primitive meteorites: Insights from mineral separation and partial dissolution.
152 Geochimica et Cosmochimica Acta 156, 1-24.
153 Greenwood, R.C., Barrat, J.-A., Miller, M.F., Anand, M., Dauphas, N., Franchi, I.A.,
154 Sillard, P. and Starkey, N.A. (2018) Oxygen isotopic evidence for accretion of Earth's
155 water before a high-energy Moon-forming giant impact. Science advances 4, eaao5928.
156 Greenwood, R.C., Burbine, T.H., Miller, M.F. and Franchi, I.A. (2017) Melting and

differentiation of early-formed asteroids: The perspective from high precision oxygen isotope studies. Chemie der Erde 77, 1-43.
Greenwood, R.C., Franchi, I.A., Kearsley, A.T. and Alard, O. (2010) The relationship between CK and CV chondrites. Geochimica et Cosmochimica Acta 74, 1684-1705.
Harries, D. and Bischoff, A. (2020) Petrological evidence for the existence and disruption of a 500 km-sized differentiated planetesimal of enstatite-chondritic parentage. Earth and Planetary Science Letters 548, 116506.
Holden, N.E. (1990) Total half-lives for selected nuclides. Pure and Applied Chemistry 62, 941-958.
Inglis, E.C., Creech, J.B., Deng, Z. and Moynier, F. (2018) High-precision zirconium stable isotope measurements of geological reference materials as measured by double-spike MC-ICPMS. Chemical Geology 493, 544-552.
Ireland, T.R., Avila, J., Greenwood, R.C., Hicks, L.J. and Bridges, J.C. (2020) Oxygen Isotopes and Sampling of the Solar System. Space Science Reviews 216, 25.
Jerram, M., Bonnand, P., Kerr, A.C., Nisbet, E.G., Puchtel, I.S. and Halliday, A.N. (2020) The δ53Cr isotope composition of komatiite flows and implications for the composition of the bulk silicate Earth. Chemical Geology 551, 119761.
Johansen, A., Low, M.-M.M., Lacerda, P. and Bizzarro, M. (2015) Growth of asteroids, planetary embryos, and Kuiper belt objects by chondrule accretion. Science Advances 1, e1500109.
Keil, K. (1968) Mineralogical and chemical relationships among enstatite chondrites. Journal of Geophysical Research (1896-1977) 73, 6945-6976.
Keil, K. (1989) Enstatite meteorites and their parent bodies. Meteoritics 24, 195-208.
Keil, K. (2010a) Enstatite achondrite meteorites (aubrites) and the histories of their asteroidal parent bodies. Geochemistry 70, 295-317.
Keil, K. (2010b) Enstatite achondrite meteorites (aubrites) and the histories of their asteroidal parent bodies. Chemie der Erde-Geochemistry 70, 295-317.
Keil, K. and Bischoff, A. (2008) Northwest Africa 2526: A partial melt residue of enstatite chondrite parentage. Meteoritics and Planetary Science 43, 1233-1240.
Keil, K., Ntaflos, T., Taylor, G., Brearley, A., Newsom, H. and Romig Jr, A. (1989) The Shallowater aubrite: Evidence for origin by planetesimal impacts. Geochimica et Cosmochimica Acta 53, 3291-3307.
Larsen, K.K., Wielandt, D. and Bizzarro, M. (2018) Multi-element ion-exchange chromatography and high-precision MC-ICP-MS isotope analysis of Mg and Ti from sub-mm-sized meteorite inclusions. Journal of Analytical Atomic Spectrometry 33, 613-628.
Larsen, K.K., Wielandt, D., Schiller, M. and Bizzarro, M. (2016) Chromatographic speciation of Cr(III)-species, inter-species equilibrium isotope fractionation and improved chemical purification strategies for high-precision isotope analysis. Journal of Chromatography A 1443, 162-174.
Li, S., Yin, Q.-Z., Bao, H., Sanborn, M.E., Irving, A., Ziegler, K., Agee, C., Marti, K., Miao, B., Li, X., Li, Y. and Wang, S. (2018) Evidence for a multilayered internal

199 structure of the chondritic acapulcoite-lodranite parent asteroid. Geochimica et
200 Cosmochimica Acta 242, 82-101.
201 Liu, C.Y., Xu, L.J., Liu, C.T., Liu, J., Qin, L.P., Zhang, Z.D., Liu, S.A. and Li, S.G.
202 (2019) High-Precision Measurement of Stable Cr Isotopes in Geological Reference
203 Materials by a Double-Spike TIMS Method. Geostandards and Geoanalytical Research
204 43, 647-661.
205 Lodders, K. (2003) Solar system abundances and condensation temperatures of the
206 elements. The Astrophysical Journal 591, 1220-1247.
207 Lodders, K., Palme, H. and Wlotzka, F. (1993) Trace elements in mineral separates of
208 the Pena Blanca Spring aubrite: Implications for the evolution of the aubrite parent
209 body. Meteoritics 28, 538-551.
210 Lorenzetti, S., Eugster, O., Busemann, H., Marti, K., Burbine, T.H. and McCoy, T.
211 (2003) History and origin of aubrites. Geochimica et Cosmochimica Acta 67, 557-571.
212 Lugmair, G. and Shukolyukov, A. (1998) Early solar system timescales according to
213 ^{53}Mn-^{53}Cr systematics. Geochimica et Cosmochimica Acta 62, 2863-2886.
214 Miura, Y.N., Hidaka, H., Nishiizumi, K. and Kusakabe, M. (2007) Noble gas and
215 oxygen isotope studies of aubrites: A clue to origin and histories. Geochimica et
216 cosmochimica acta 71, 251-270.
217 Mougel, B., Moynier, F. and Göpel, C. (2018) Chromium isotopic homogeneity
218 between the Moon, the Earth, and enstatite chondrites. Earth and Planetary Science
219 Letters 481, 1-8.
220 Moynier, F., Deng, Z., Lanteri, A., Martins, R., Chaussidon, M., Savage, P. and Siebert,
221 J. (2020) Metal-silicate silicon isotopic fractionation and the composition of the bulk
222 Earth. Earth and Planetary Science Letters 549, 116468.
223 Moynier, F., Paniello, R.C., Gounelle, M., Albarède, F., Beck, P., Podosek, F. and Zanda,
224 B. (2011a) Nature of volatile depletion and genetic relationships in enstatite chondrites
225 and aubrites inferred from Zn isotopes. Geochimica et Cosmochimica Acta 75,
226 297-307.
227 Moynier, F., Yin, Q.-Z. and Schauble, E. (2011b) Isotopic evidence of Cr partitioning
228 into Earth's core. Science 331, 1417-1420.
229 Newton, J., Franchi, I.A. and Pillinger, C.T. (2000) The oxygen-isotopic record in
230 enstatite meteorites. Meteoritics & Planetary Science 35, 689-698.
231 Nittler, L.R. and Weider, S.Z. (2019) The surface composition of Mercury. Elements:
232 An International Magazine of Mineralogy, Geochemistry, and Petrology 15, 33-38.
233 Patzer, A., Hill, D.H. and Boynton, W.V. (2001) Itqiy: A metal-rich enstatite meteorite
234 with achondritic texture. Meteoritics and Planetary Science 36, 1495-1505.
235 Patzer, A., Hill, D.H., Boynton, W.V., Franke, L., Schultz, L., Jull, A.J.T., McHargue,
236 L.R. and Franchi, I.A. (2002) Itqiy: A study of noble gases and oxygen isotopes
237 including its terrestrial age and a comparison with Zakłodzie. Meteoritics and Planetary
238 Science 37, 823-833.
239 Pedersen, S.G., Schiller, M., Connelly, J.N. and Bizzarro, M. (2019) Testing accretion
240 mechanisms of the H chondrite parent body utilizing nucleosynthetic anomalies.

Meteoritics & Planetary Science 54, 1215-1227.
Petitat, M., Birck, J.-L., Luu, T. and Gounelle, M. (2011) The chromium isotopic composition of the ungrouped carbonaceous chondrite Tagish Lake. The Astrophysical Journal 736, 23.
Piani, L., Marrocchi, Y., Rigaudier, T., Vacher, L.G., Thomassin, D. and Marty, B. (2020) Earth's water may have been inherited from material similar to enstatite chondrite meteorites. Science 369, 1110-1113.
Pravdivtseva, O., Meshik, A., Hohenberg, C. and Krot, A. (2017) I–Xe systematics of the impact plume produced chondrules from the CB carbonaceous chondrites: Implications for the half-life value of 129I and absolute age normalization of ^{129}I–^{129}Xe chronometer. Geochimica et cosmochimica acta 201, 320-330.
Qin, L., Alexander, C.M.O.D., Carlson, R.W., Horan, M.F. and Yokoyama, T. (2010) Contributors to chromium isotope variation of meteorites. Geochimica et Cosmochimica Acta 74, 1122-1145.
Rubin, A.E. (2015) Impact features of enstatite-rich meteorites. Geochemistry 75, 1-28.
Schiller, M., Baker, J., Creech, J., Paton, C., Millet, M.-A., Irving, A. and Bizzarro, M. (2011) Rapid timescales for magma ocean crystallization on the howardite-eucrite-diogenite parent body. The Astrophysical Journal Letters 740, L22.
Schiller, M., Connelly, J.N., Glad, A.C., Mikouchi, T. and Bizzarro, M. (2015) Early accretion of protoplanets inferred from a reduced inner solar system 26Al inventory. Earth and Planetary Science Letters 420, 45-54.
Schiller, M., Van Kooten, E., Holst, J.C., Olsen, M.B. and Bizzarro, M. (2014) Precise measurement of chromium isotopes by MC-ICPMS. Journal of analytical atomic spectrometry 29, 1406-1416.
Schneider, J.M., Burkhardt, C., Marrocchi, Y., Brennecka, G.A. and Kleine, T. (2020) Early evolution of the solar accretion disk inferred from Cr-Ti-O isotopes in individual chondrules. Earth and Planetary Science Letters 551, 116585.
Schoenberg, R., Merdian, A., Holmden, C., Kleinhanns, I.C., Haßler, K., Wille, M. and Reitter, E. (2016) The stable Cr isotopic compositions of chondrites and silicate planetary reservoirs. Geochimica et Cosmochimica Acta 183, 14-30.
Schoenberg, R., Zink, S., Staubwasser, M. and Von Blanckenburg, F. (2008) The stable Cr isotope inventory of solid Earth reservoirs determined by double spike MC-ICP-MS. Chemical Geology 249, 294-306.
Schrader, D.L., Franchi, I.A., Connolly, H.C., Greenwood, R.C., Lauretta, D.S. and Gibson, J.M. (2011) The formation and alteration of the Renazzo-like carbonaceous chondrites I: Implications of bulk-oxygen isotopic composition. Geochimica et Cosmochimica Acta 75, 308-325.
Sedaghatpour, F. and Teng, F.-Z. (2016) Magnesium isotopic composition of achondrites. Geochimica et Cosmochimica Acta 174, 167-179.
Shahar, A., Hillgren, V.J., Horan, M.F., Mesa-Garcia, J., Kaufman, L.A. and Mock, T.D. (2015) Sulfur-controlled iron isotope fractionation experiments of core formation in planetary bodies. Geochimica et Cosmochimica Acta 150, 253-264.

283 Shen, J., Liu, J., Qin, L., Wang, S.J., Li, S., Xia, J., Ke, S. and Yang, J. (2015)
284 Chromium isotope signature during continental crust subduction recorded in
285 metamorphic rocks. Geochemistry, Geophysics, Geosystems 16, 3840-3854.
286 Shen, J., Xia, J., Qin, L., Carlson, R.W., Huang, S., Helz, R.T. and Mock, T.D. (2019)
287 Stable chromium isotope fractionation during magmatic differentiation: Insights from
288 Hawaiian basalts and implications for planetary redox conditions. Geochimica et
289 Cosmochimica Acta.
290 Shima, M. and Honda, M. (1966) Distribution of spallation produced chromium
291 between alloys in iron meteorites. Earth and Planetary Science Letters 1, 65-74.
292 Shukolyukov, A. and Lugmair, G.W. (2004) Manganese-chromium isotope systematics
293 of enstatite meteorites. Geochimica et Cosmochimica Acta 68, 2875-2888.
294 Sossi, P., Moynier, F. and van Zuilen, K. (2018) Volatile loss following cooling and
295 accretion of the Moon revealed by chromium isotopes. Proceedings of the National
296 Academy of Sciences 115, 10920-10925.
297 Sossi, P.A., Klemme, S., O'Neill, H.S.C., Berndt, J. and Moynier, F. (2019) Evaporation
298 of moderately volatile elements from silicate melts: experiments and theory.
299 Geochimica et Cosmochimica Acta 260, 204-231.
300 Stracke, A., Palme, H., Gellissen, M., Münker, C., Kleine, T., Birbaum, K., Günther, D.,
301 Bourdon, B. and Zipfel, J. (2012) Refractory element fractionation in the Allende
302 meteorite: Implications for solar nebula condensation and the chondritic composition of
303 planetary bodies. Geochimica et Cosmochimica Acta 85, 114-141.
304 Trinquier, A., Birck, J.-L. and Allègre, C.J. (2007) Widespread 54Cr heterogeneity in
305 the inner solar system. The Astrophysical Journal 655, 1179-1185.
306 Trinquier, A., Birck, J.-L. and Allègre, C.J. (2008a) High-precision analysis of
307 chromium isotopes in terrestrial and meteorite samples by thermal ionization mass
308 spectrometry. Journal of Analytical Atomic Spectrometry 23, 1565-1574.
309 Trinquier, A., Birck, J.L., Allègre, C.J., Göpel, C. and Ulfbeck, D. (2008b) 53Mn–53Cr
310 systematics of the early Solar System revisited. Geochimica et Cosmochimica Acta 72,
311 5146-5163.
312 Udry, A., Wilbur, Z.E., Rahib, R.R., McCubbin, F.M., Vander Kaaden, K.E., McCoy,
313 T.J., Ziegler, K., Gross, J., DeFelice, C., Combs, L. and Turrin, B.D. (2019)
314 Reclassification of four aubrites as enstatite chondrite impact melts: Potential
315 geochemical analogs for Mercury. Meteoritics & Planetary Science 54, 785-810.
316 van Acken, D., Brandon, A.D. and Lapen, T.J. (2012a) Highly siderophile element and
317 osmium isotope evidence for postcore formation magmatic and impact processes on the
318 aubrite parent body. Meteoritics & Planetary Science 47, 1606-1623.
319 van Acken, D., Humayun, M., Brandon, A.D. and Peslier, A.H. (2012b) Siderophile
320 trace elements in metals and sulfides in enstatite achondrites record planetary
321 differentiation in an enstatite chondritic parent body. Geochimica et Cosmochimica
322 Acta 83, 272-291.
323 Van Kooten, E.M.M.E., Schiller, M. and Bizzarro, M. (2017) Magnesium and
324 chromium isotope evidence for initial melting by radioactive decay of 26Al and late

stage impact-melting of the ureilite parent body. Geochimica et Cosmochimica Acta 208, 1-23.
Van Kooten, E.M.M.E., Wielandt, D., Schiller, M., Nagashima, K., Thomen, A., Larsen, K.K., Olsen, M.B., Nordlund, Å., Krot, A.N. and Bizzarro, M. (2016) Isotopic evidence for primordial molecular cloud material in metal-rich carbonaceous chondrites. Proceedings of the National Academy of Sciences 113, 2011-2016.
Verkouteren, R.M. and Lipschutz, M.E. (1983) Cumberland Falls chondritic inclusions—II. Trace element contents of forsterite chondrites and meteorites of similar redox state. Geochimica et Cosmochimica Acta 47, 1625-1633.
Vermeesch, P. (2018) IsoplotR: A free and open toolbox for geochronology. Geoscience Frontiers 9, 1479-1493.
Wang, K., Savage, P.S. and Moynier, F. (2014) The iron isotope composition of enstatite meteorites: Implications for their origin and the metal/sulfide Fe isotopic fractionation factor. Geochimica et Cosmochimica Acta 142, 149-165.
Warren, P.H. (2011) Stable-isotopic anomalies and the accretionary assemblage of the Earth and Mars: A subordinate role for carbonaceous chondrites. Earth and Planetary Science Letters 311, 93-100.
Wasson, J.T. (1988) The building stones of the planets. Mercury, University of Arizona Press, 622-650.
Watters, T.R. and Prinz, M. (1979) Aubrites-Their origin and relationship to enstatite chondrites, Proceedings of the 10th Lunar and Planetary Science Conference.
Wilson, L. and Keil, K. (1991) Consequences of explosive eruptions on small solar system bodies: The case of the missing basalts on the aubrite parent body. Earth and Planetary Science Letters 104, 505-512.
Wood, B.J., Kiseeva, E.S. and Mirolo, F.J. (2014) Accretion and core formation: The effects of sulfur on metal–silicate partition coefficients. Geochimica et Cosmochimica Acta 145, 248-267.
Wood, B.J., Wade, J. and Kilburn, M.R. (2008) Core formation and the oxidation state of the Earth: Additional constraints from Nb, V and Cr partitioning. Geochimica et Cosmochimica Acta 72, 1415-1426.
Wu, G., Zhu, J.-M., Wang, X., Johnson, T.M. and Han, G. (2020) High-Sensitivity Measurement of Cr Isotopes by Double Spike MC-ICP-MS at the 10 ng Level. Analytical Chemistry 92, 1463-1469.
Yamakawa, A., Yamashita, K., Makishima, A. and Nakamura, E. (2010) Chromium isotope systematics of achondrites: Chronology and isotopic heterogeneity of the inner solar system bodies. The Astrophysical Journal 720, 150.
Yamashita, K., Maruyama, S., Yamakawa, A. and Nakamura, E. (2010) ^{53}Mn-^{53}Cr chronometry of CB chondrite: Evidence for uniform distribution of 53Mn in the early solar system. The Astrophysical Journal 723, 20.
Zhang, J., Dauphas, N., Davis, A.M., Leya, I. and Fedkin, A. (2012) The proto-Earth as a significant source of lunar material. Nature Geosci 5, 251-255.
Zhu, K., Liu, J., Moynier, F., Qin, L., Alexander, C.M.O.D. and He, Y. (2019a)

Chromium isotopic evidence for an early formation of chondrules from the Ornans CO chondrite. The Astrophysical Journal 873, 82.

Zhu, K., Moynier, F., Barrat, J.-A., Wielandt, D., Larsen, K. and Bizzarro, M. (2019b) Timing and origin of the angrite parent body inferred from Cr isotopes. The Astrophysical Journal Letters 877, L13.

Zhu, K., Moynier, F., Schiller, M., Alexander, C.M.O.D., Barrat, J.-A., Bischoff, A. and Bizzarro, M. (2021a) Mass–independent and mass–dependent Cr isotopic composition of the Rumuruti (R) chondrites: Implications for their origin and planet formation. Geochimica et Cosmochimica Acta 293, 598-609.

Zhu, K., Moynier, F., Schiller, M., Alexander, C.M.O.D., Davidson, J., Schrader, D.L., van Kooten, E.M.M.E. and Bizzarro, M. (2021b) Chromium isotopic insights into the origin of chondrite parent bodies and the early terrestrial volatile depletion. Geochimica et Cosmochimica Acta 301, 158-186.

Zhu, K., Moynier, F., Schiller, M. and Bizzarro, M. (2020a) Dating and tracing the origin of enstatite chondrite chondrules with Cr isotopes. The Astrophysical Journal Letters 894, L26.

Zhu, K., Moynier, F., Schiller, M., Wielandt, D., Larsen, K., van Kooten, E. and Bizzarro, M. (2020b) Chromium isotopic constraints on the origin the ureilite parent body. The Astrophysical Journal 888, 126.

Zhu, K., Sossi, P.A., Siebert, J. and Moynier, F. (2019c) Tracking the volatile and magmatic history of Vesta from chromium stable isotope variations in eucrite and diogenite meteorites. Geochimica et Cosmochimica Acta 266, 598-610.